

## Signature of high-amplitude pulsations in seven $\delta$ Sct stars via TESS observations

FATEMEH VASIGH,<sup>1</sup> ELHAM ZIAALI,<sup>1,2</sup> AND HOSSEIN SAFARI<sup>1,3</sup>

<sup>1</sup>*Department of Physics, Faculty of Science, University of Zanjan, University Blvd., Zanjan, 45371-38791, Zanjan, Iran*

<sup>2</sup>*Instituto de Astrofísica de Andalucía – CSIC, E-18008 Granada, Spain*

<sup>3</sup>*Observatory, Faculty of Science, University of Zanjan, University Blvd., Zanjan, 45371-38791, Zanjan, Iran*

### ABSTRACT

The regular behavior of the pulsations of high-amplitude  $\delta$  Sct (HADS) stars gives a greater chance to investigate the interiors of stars. We analyzed seven HADS stars showing peak-to-peak amplitudes of more than 0.3 mag that were newly observed by TESS. We obtained that TIC 374753270, TIC 710783, and TIC 187386415 pulsate in fundamental radial mode; also, TIC 130474019 and TIC 160120432 show double radial modes. On the other hand, TIC 148357344 and TIC 278119167 demonstrate triple-mode behavior. Our analysis shows that these seven stars are close to the red edge of the (inside) instability strip in the Hertzsprung–Russell diagram. The fundamental mode of these seven targets follows the period-luminosity (PL) relation for  $\delta$  Sct stars. However, TIC 278119167 deviates slightly from the fundamental PL relation. The double-mode and triple-mode HADS stars (TIC 130474019, TIC 160120432, TIC 148357344, and TIC 278119167) are in agreement with the period ratio ranges (fundamental to first and second overtones). Using the information of 176 HADS stars (Netzel and Smolec), we find a scaling relation ( $[\text{Fe}/\text{H}] \propto \log(M^{7.95 \pm 0.15} L^{-1.83 \pm 0.11} P_0^{0.79 \pm 0.14} T_{\text{eff}}^{0.047 \pm 0.02})$ ) between the metallicity ( $[\text{Fe}/\text{H}]$ ) and mass ( $M$ ), luminosity ( $L$ ), effective temperature ( $T_{\text{eff}}$ ), and the fundamental period ( $P_0$ ). We estimate the metallicity of the seven newly identified HADS stars ranging from -0.62 to 0.37 dex.

*Keywords:* Asteroseismology (73); Delta Scuti variable stars (370); Stellar oscillations (1617)

### 1. INTRODUCTION

Asteroseismology is an approach to studying the internal characteristics of pulsating stars through their oscillation modes (Aerts et al. 2010; Antoci et al. 2019; Bedding et al. 2020; Holdsworth et al. 2024). The asteroseismology approach has more details explanations for the interior structure of different stars by increasing the resolution (temporal, spectral, and spatial) of ground and space observations of the pulsating stars. While overall instrument resolution (temporal and spatial) helps measure pulsation frequencies more precisely, the spectral resolution provides extra detail of chemical abundances (metallicity). Studies of Kepler (Gilliland et al. 2010) data have had significant impacts on asteroseismology. Recently, the Transiting Exoplanet Survey Satellite (TESS; Ricker et al. (2015)) provided unprecedented space observations of numerous star systems. Antoci et al. (2019) reported the information of 117  $\delta$  Sct stars from TESS short-cadence observations for sectors 1 and 2. Very recently, Read et al. (2024) identified 848  $\delta$  Sct stars having a narrow color range of  $0.29 < G_{BP} - G_{RP} < 0.31$  (at the center of instability strip) as being nearer than 500 pc by using sectors 27-55 of TESS observations and Gaia Data Release 3 (DR3) information. Investigating the pulsation property of  $\delta$  Sct stars could help to understand their internal structure, such as rotation, chemical composition, density, temperature, and gravity.

In the Hertzsprung–Russell (H-R) diagram,  $\delta$  Sct stars are pulsating variables of spectral types A0-F5 that mainly lie at the overlap of the main sequence and the instability strip (Breger 1979; Murphy et al. 2020; Bowman & Michielsen 2021). The  $\delta$  Sct stars have the intermediate mass located at the transition region from low-mass to high-mass stars. Stars with lower than 1 and higher than 2  $M_{\odot}$  are called low-mass and high-mass, respectively. The effective temperature range of the  $\delta$  Sct stars lies between 6500 and 9500 K (Petersen & Christensen-Dalsgaard 1996; Breger 2000a; McNamara 2011; Bowman et al. 2016; Pietrukowicz et al. 2020; Murphy et al. 2019; Jayasinghe et al. 2020; Yang et al. 2021b). The  $\delta$  Sct stars pulsation frequencies are in the range of

Corresponding author: Elham ZIAALI, Hossein SAFARI

ziaali@znu.ac.ir

safari@znu.ac.ir

5-60 day<sup>-1</sup>. They show various modes of pulsations such as radial, nonradial pressure modes, and mixed modes of the low radial order in their complex light curves (Houdek et al. 1999; Breger 2000b; Handler 2009; Hasanzadeh et al. 2021; Soszyński et al. 2021)

Their pulsations are primarily driven by the classical  $\kappa$  mechanism in the He II ionization zone. Some studies also suggested that intrinsically stable, stochastically driven (solar-like)  $p$ -modes may be excited simultaneously in such  $\delta$  Sct star (Baker & Kippenhahn 1962; Balmforth & Gough 1990; Houdek et al. 1999; Samadi et al. 2002; Antoci et al. 2011; Antoci 2013).

High-amplitude  $\delta$  Sct (HADS) stars pulsate in  $V$ -band amplitudes over 0.3 mag. However, there are few reports on HADS stars showing peak-to-peak value slightly smaller than 0.3 mag (Breger et al. 2011; Lv et al. 2023). HADS stars are characterized by their high amplitude, short periods (less than one day), and also  $v \sin i \leq 30 \text{ km s}^{-1}$ . HADS stars oscillate as single-periodic with a radial fundamental mode or double-periodic or triple-periodic pulsators (Bono et al. 1997; Wils et al. 2008; McNamara 2011; Yang et al. 2021a; Netzel & Smolec 2022; Lv et al. 2023; Xue et al. 2023). However, the number of HADS stars having four independent radial frequencies as quadruple-mode HADS stars has been increasing in recent years (Mow et al. 2016; Lv et al. 2022).

Also, nonradial modes may exist in the HADS frequency spectrum (Uytterhoeven et al. 2011). HADS stars are important because they can be used to study the structure and evolution of stars. These stars can be used to investigate the evolution of stellar populations, as they are found in old stellar populations, while low-amplitude  $\delta$  Sct (LADS) stars are young and intermediate-age stars (Chang et al. 2013; Netzel & Smolec 2022; Soszyński et al. 2021). Recently, there has been a growing interest in HADS stars as potential targets for exoplanet searches. High-precision observations of HADS stars' pulsations and signatures of orbiting planets could detect slight variations in their light curves. Several exoplanets have already been discovered around HADS stars (Hey et al. 2021; Guzik 2021). Lv et al. (2023) studied seven new HADS stars through photometric data of TESS and reported that two stars may be RR Lyrae based on their light curves and the difference in their placement with the HADS star in the Peterson and period-luminosity (PL) diagrams. In these HADS stars, the metallicity can have a greater effect than the rotation of the star on the period ratios (the ratio of overtones to the fundamental mode). The period ratios decrease with increasing metallicity.

Metallicity is often expressed as a ratio of the abundance of iron (Fe) to hydrogen (H) compared to the solar ratio, written as [Fe/H] (Kotoneva et al. 2002; Chruslinska & Nelemans 2019). A metallicity value greater than -0.5 dex indicates metal-rich  $\delta$  Sct stars, while a value less than -1.5 dex shows a metal-poor star (McNamara 2011). Determining a star's metallicity involves sophisticated astronomical techniques based on spectroscopic investigations (Lianou et al. 2011; Liu et al. 2020), photometric methods (Li et al. 2023; Dékány & Grebel 2022) and astroseismology approach (Netzel & Smolec 2022).

Here, we analyzed the light curves of seven newly identified HADS stars from TESS observations. We selected these HADS from the TESS catalog of several thousand of  $\delta$  Sct stars applying three criteria: (1) the peak-to-peak amplitude is greater than 0.3 mag, (2) the related extinction is less than 0.6 mag, and (3) the relative parallax error is less than 0.05. Therefore, we applied more analyses to seven HADS having short-cadence TESS observation that satisfied the above criteria for more asteroseismic analyses. To do this, we extracted the frequencies and amplitudes of these seven stars using the periodogram analysis.

We studied the PL behavior and H-R diagram. To determine the metallicity of targets, we obtained a scaling relation between the metallicity of 176 HADS stars (Netzel & Smolec 2022) and their physical parameters (mass, luminosity, and effective temperature) and the fundamental periods. Section 2 gives the HADS star information used in this paper. Sections 3 and 4 explain the methods and results, respectively. Finally, section 5 summarizes the essential findings of the present work.

## 2. DATA

TESS is a space mission for probing exoplanets (Ricker et al. (2015)). This telescope divides the sky into sectors and observes each sector for 27 days. The TESS space telescope was designed to record objects in a red passband of approximately 600–1000 nm (Aguirre et al. 2015; Barclay et al. 2018). TESS data are available in two forms, target pixel file (TPF) and light curve, which can be searched applying the Lightkurve tool (Lightkurve Collaboration et al. 2018). Figure 1 illustrates TPF and aperture (red squares) for TIC 374753270 (left, first row), TIC 130474019 (right, first row), TIC 148357344 (left, second row), TIC 160120432 (right, second row), TIC 278119167 (left, third row), TIC 710783 (right, third row), and TIC 187386415 (fourth row). As shown in the figure, each aperture covers the primary pixels of each target without considerable contamination of another object in the field of view. In this paper, we used photometric data processed by SPOC (Jenkins et al. 2016), which are short-cadence (2 minutes). We transformed the flux to magnitude and subtracted from its average value for each light curve to get the corrected time series.

<http://dx.doi.org/10.17909/4a25-pg87>

## 3. METHOD

**Table 1.** TIC number, variable name, and TESS short-cadence sector(s) for seven HADS stars.

TIC	Star Name	Sector
374753270	-	36,37
130474019	-	7, 34
148357344	-	7
160120432	YZ UMi	14, 19, 20, 40, 47, 52, 53
278119167	-	40, 53
710783	-	5
187386415	-	51

### 3.1. Frequency analysis

We selected seven  $\delta$  Sct light curves (related to TPFs of Figure 1) with peak-to-peak amplitudes greater than 0.3 mag as an essential characteristic for identifying HADS stars. We checked the TPFs for each target to ensure the SPOC light curve's validity due to the SPOC aperture's size, which would not be contaminated by the neighbor objects in the field. Our investigation showed that the SPOC light curves were perfect for our targets. Then, their SPOC-prepared light curves were analyzed to extract pulsation frequencies. We removed outliers from each star's light curve. We rejected the outlier data points from light curves (data points were far from the average). We first calculated the average and standard deviation for each light curve. The outlier data points have amplitudes more significant than 4 standard deviations ( $4\sigma$ ). Also, the mean of each single light curve was subtracted to get the corrected systematic error flux. To study our samples' pulsating behavior, the PERIOD04 (Lenz & Breger 2005) software was applied. A prewhitening procedure carried out the frequency extraction. The Nyquist frequency is half of the sampling rate,  $f_N = 360.048 \text{ day}^{-1}$  for 2 minute cadence observations. This value is well above the limit range ( $5 < f < 60 \text{ day}^{-1}$ ) expected for a typical  $\delta$  Sct star pulsation. We used a resolution frequency  $f_{res} = 1.5/\Delta T$  to identify nearby frequencies in the amplitude spectrum, where  $\Delta T$  represents the length of the light curve (Loumos & Deeming 1978). Two frequencies are resolved if the frequency difference is more than the resolution frequency. The light curves are modeled by

$$m = m_0 + \sum_{i=1}^N A_i \sin(2\pi(f_i t + \phi_i)), \quad (1)$$

where  $m_0$  is the zero point,  $A_i$  is the amplitude,  $f_i$  is the frequency, and  $\phi_i$  is the phase.

The PERIOD04 algorithm gives the frequency, amplitude, and phase of each significant mode by applying the multifrequency least-square fit (Equation 1) for the stellar light curve. We considered the modes with a signal-to-noise ratio (S/N) more significant than 5.2 (Baran et al. 2015). The residual is determined by subtracting the modeled light curve from the original light curve that is expected to show the lack of significant modes (S/N > 5.2). The uncertainty of the peaks is determined using the approach by Montgomery & O'Donoghue (1999).

### 3.2. Asteroseismic analysis

The stellar oscillations are helpful to infer information about the stars' interior. Each mode can be described by three quantum numbers:  $n$  (radial number),  $l$  (degree), and  $m$  (azimuthal number), which are related to the characteristics of oscillations. In most pulsating stars, we expect the highest amplitude mode to be the fundamental radial ( $n = 1, l = 0$ ) oscillation (Aerts et al. 2010; Murphy et al. 2020).

The  $\delta$  Sct stars' power spectrum, the frequency corresponding to the highest peak amplitude, is called  $f_{A_{max}}$ . The  $f_{A_{max}}$  might change over time due to modulation of amplitude and other factors such as noise (Bowman 2017). Radial modes can be identified based on the ratio of their periods. Frequency (period) ratios for radial modes (fundamental (F0), first (F1), second (F2) and third (F3) overtones) were first presented by Stellingwerf (1979) based on theoretical models as  $F0/F1 = 0.756 - 0.787$ ,  $F0/F2 = 0.611 - 0.632$ , and  $F0/F3 = 0.50 - 0.525$ .

For  $\delta$  Sct stars with the first and the second overtones, the characteristic frequency (period) ratios are around  $F1/F2 = 0.8$  (Soszyński et al. 2021). The combination of different frequencies or the linear sum of the independent frequencies,  $nv_i \pm mv_j$ , was identified by the Loumos & Deeming (1978) criteria. The modes with no agreement with combination or harmonic frequencies might be identified as nonradial modes. Whereas the frequency (period) of pulsations is linked to stars' interior characteristics,

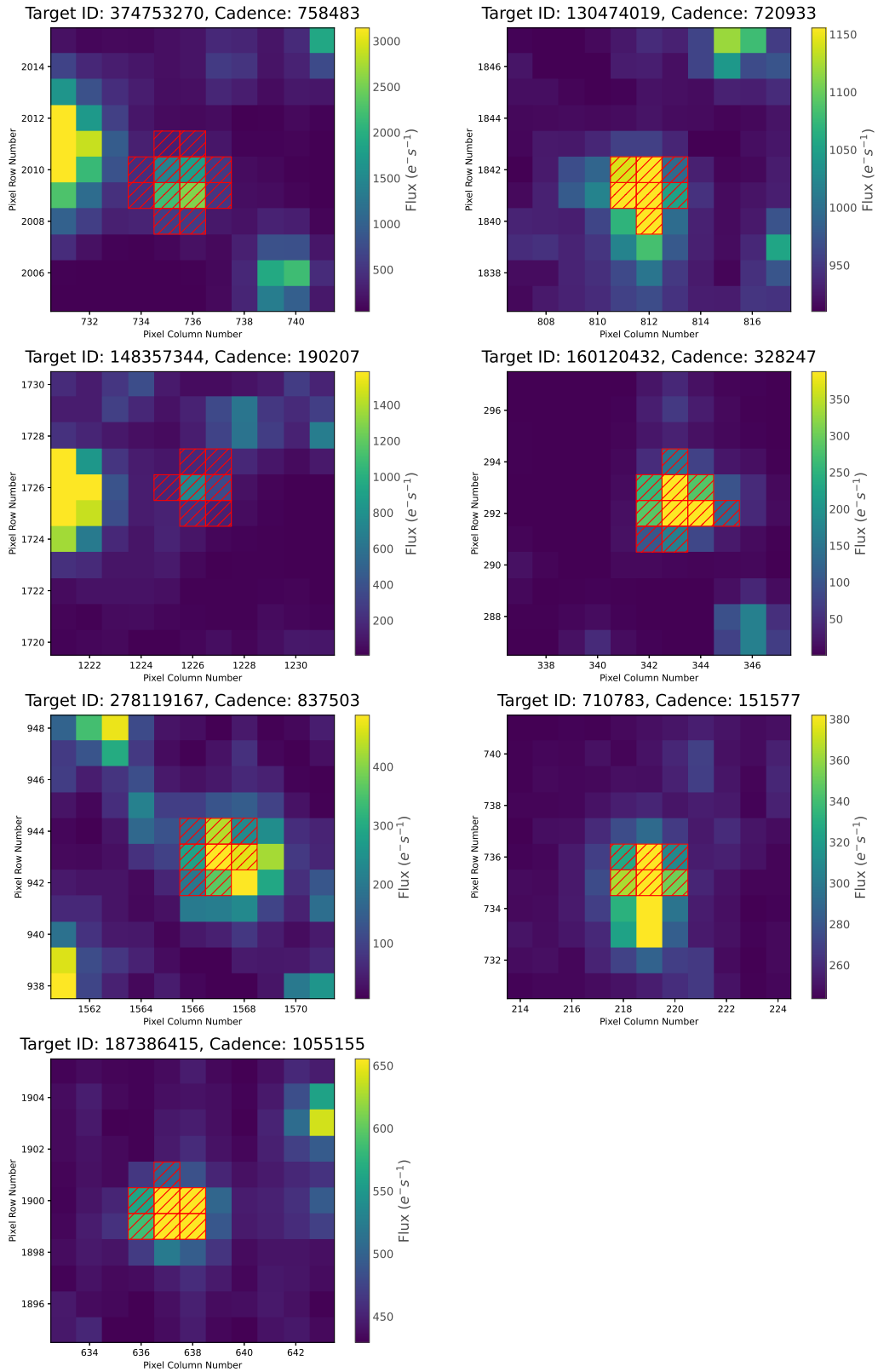


**Figure 1.** Target Pixel File (TPF) for TIC 374753270 (left-first row), TIC 130474019 (right-first row), TIC 148357344 (left-second row), TIC 160120432 (right-second row), TIC 278119167 (left-third row), TIC 710783 (right-third row), and TIC 187386415 (fourth-row). The aperture for each target star is indicated by the red squares.

the frequency is related to the radius changes. The critical factor is the density of stars that is accurately related to the period. The period-density relation is defines as

$$Q = P\sqrt{\bar{\rho}/\bar{\rho}_{\odot}}, \quad (2)$$

where  $\bar{\rho}$  describes the mean densities of the target star and  $\bar{\rho}_{\odot}$  is the mean density for Sun.  $P$  is the pulsation period. The other forms of Equation (2) were given by Breger (1990) that included the gravity acceleration and bolometric magnitudes. Here, we used Equation (2) to validate the periods of seven targets. The range of pulsations constant ( $Q$ ) for  $\delta$  Sct stars' fundamental, first, second, and third overtone frequencies are 0.027 – 0.04, 0.021 – 0.027, 0.018 – 0.021, and 0.016 – 0.017, respectively (Breger & Bregman 1975; Milligan & Carson 1992).

### 3.2.1. Period–Luminosity relation

The PL relation is a dependency between the star's luminosity and density. Consequently, this relation occurs between the luminosity and the pulsation period of a group of pulsating stars that have a relatively narrow range of effective temperature. The first PL was given by Leavitt & Pickering (1912) for Cepheid stars. We computed the absolute  $V$ -band magnitudes ( $M_V$ ) for our seven targets using the following equation:

$$M_V = m_v + 5 \log \pi + 5 - A_V, \quad (3)$$

where  $m_v$  is the apparent magnitude in the  $V$  band and  $\pi$  denotes the star's parallax (in arcseconds) collected from Gaia DR3. Since interstellar dust can impact the flux of stars (luminosity), the  $M_V$  values were corrected for extinction ( $A_V$ ). Following Green et al. (2018), we determined the extinction for our seven targets to correct the  $V$ -band magnitudes. All seven samples have absolute relative parallax error (the ratio of parallax uncertainty to the parallax) in the range of 0.010-0.020 and extinctions less than 0.6 mag. By applying the Tycho  $V_T$  and  $B_T$  magnitudes, we calculated the Johnson  $V$  apparent magnitudes as (Høg et al. 2000; 1997ESA 1997),

$$V = V_T - 0.090(B_T - V_T). \quad (4)$$

We investigated the validity of the obtained fundamental frequencies by using the PL relation for our targets. Using Gaia Data Release 2 parallaxes, Ziaali et al. (2019) gave the PL relation for  $\delta$  Sct stars observed by Kepler, as follows:

$$M_V = (-2.94 \pm 0.06) \log(P) + (-1.34 \pm 0.06), \quad (5)$$

While Barac et al. (2022) reported a similar relation for stars observed by TESS using the Gaia DR3 parallaxes,

$$M_V = (-3.01 \pm 0.07) \log(P) + (-1.40 \pm 0.07). \quad (6)$$

Also, using multicolour photometric ground-based observations, Poro et al. (2021) gave

$$M_V = (-3.200 \pm 0.010) \log(P) - (1.599 \pm 0.010). \quad (7)$$

By using Equation (3) the absolute magnitude for each single star was calculated, and the PL diagram is examined (Section 4.8). These PL relations, Equations 5-7, are very close together in a narrow ridge for  $\delta$  Sct stars. So, the magnitudes and fundamental periods should be consistent with the PLs within the observational uncertainties.

## 4. RESULTS

We applied three criteria to identify the HADS stars, including the peak-to-peak amplitude more significant than 0.3 mag (from the TESS catalog), relative parallax error less than 0.05 (from Gaia DR3 catalog), and its measured extinction less than 0.6 mag. Applying the frequency analysis for the TESS light curves, we investigated the properties of the amplitude spectrum. We considered the frequencies with  $S/N > 5.2$  to ensure the validity of the identified frequencies. We obtained the period ratio and  $Q$  value. As essential criteria, if the targets (Table 1) have the  $\delta$  Sct star characteristic, we expect their absolute magnitudes and fundamental frequencies to satisfy the PL relations, Equations 5-7. Please note that these PL relations are in good agreement with the slight differences that are derived from different observations.

Figure 2 displays the position of the seven HADS stars (colored star markers) between the instability strip edges in the H-R diagram given by Murphy et al. (2019). As displayed in the figure, these seven targets tend toward the instability strip's red edge with lower temperatures. Murphy et al. (2019) investigated the instability strip boundaries based on the position of 15000  $\delta$  Sct stars in the Kepler field of view using time-dependent convection and mixing length ( $\alpha_{MLT}=1.8$ ) reported by Dupret et al. (2005). In the remainder of this paper, we examined the HADS star criteria for these seven targets.

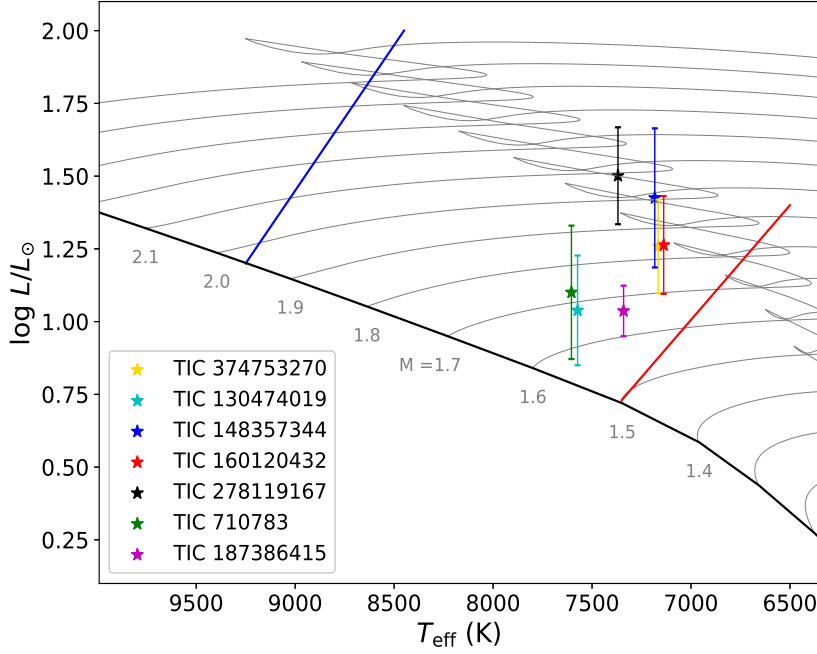


**Figure 2.** H-R diagram including our seven HADS stars indicated with different-colored star markers. The observational red and blue edge of the instability strip for  $\delta$  Sct stars along with the evolutionary tracks with  $X = 0.71$ ,  $Z = 0.014$ , and  $\alpha_{MLT}=1.8$  were obtained by [Murphy et al. \(2019\)](#). The temperatures are from [Stassun et al. \(2018\)](#) and the  $V$  band luminosities were calculated by using the apparent magnitudes, parallaxes, and the interstellar extinctions (Eq. 3). The error bars indicate the errors for luminosities.

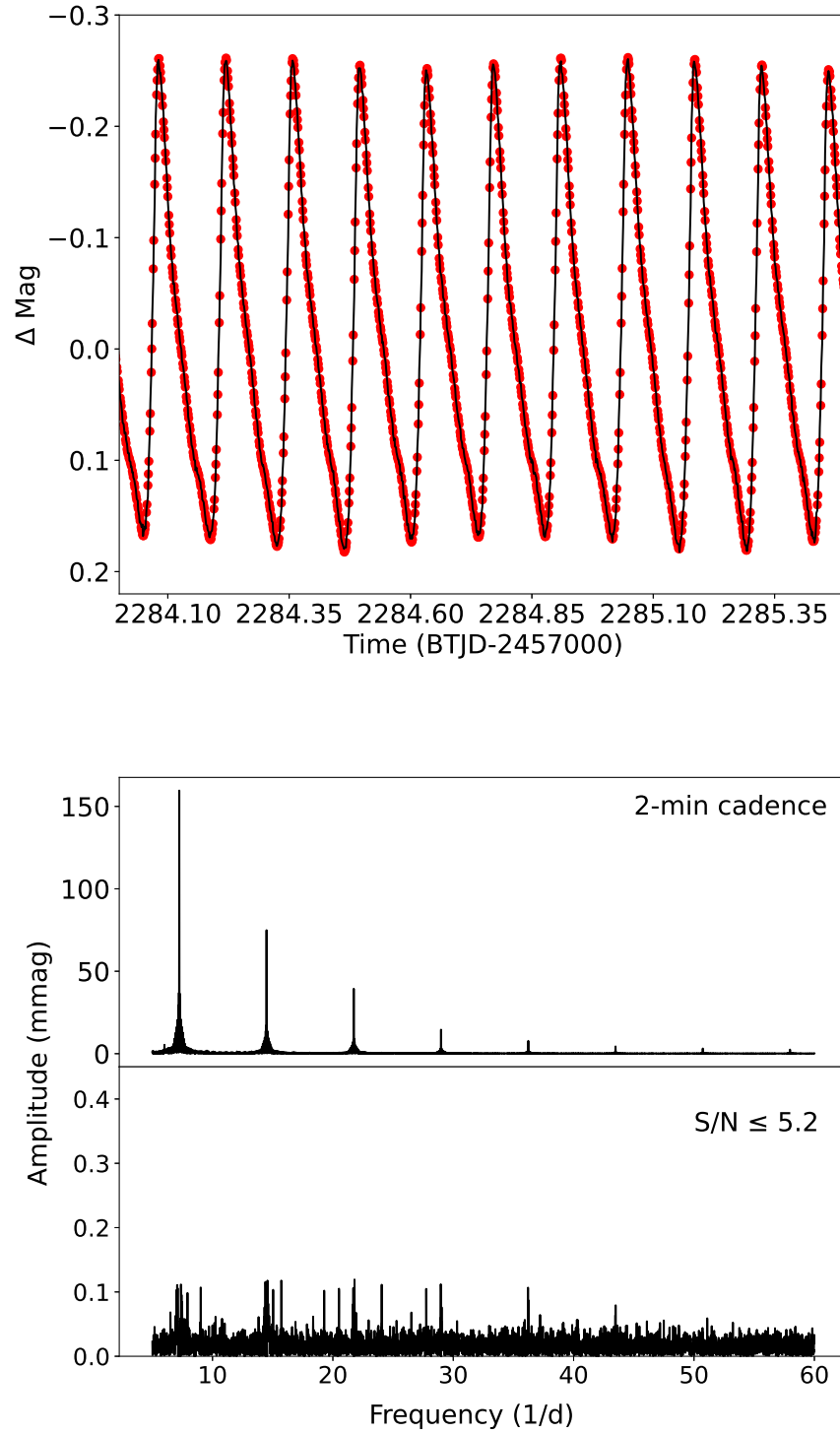
#### 4.1. TIC 374753270

Figure 3 represents the light curve (top panel), amplitude spectrum (middle panel), and amplitude spectrum of the residual (bottom panel) for TIC 374753270 (TYC 8943-3384-1). [Barac et al. \(2022\)](#) introduced TIC 374753270 ( $R.A. = 10^h03^m20^s.62$ ,  $DEC = -61^\circ51'15.63''$ ) as a  $\delta$  Sct star. We obtained the significant frequencies for combined sectors 36 and 37 using the frequency analysis approach. By frequency analysis of the combined light curve, we detected 14 significant frequencies with  $S/N > 5.2$  and frequency resolution greater than  $0.029 \text{ day}^{-1}$ . The frequencies are listed in the Table 2, including one radial frequency (monomode HADS) of  $F0 = 7.246052 \text{ day}^{-1}$  ( $P0 = 0.138$  days). Other frequencies might be called harmonics ( $f_2, f_3, f_4, f_5, f_7, f_8, f_9$ ) and nonradial modes ( $f_6, f_{10}, \dots, f_{14}$ ). These frequencies are in the reported range for  $\delta$  Sct stars ([Breger 2000a](#); [Liakos & Niarchos 2017](#)). Removing these 14 identified modes, we obtained the amplitude spectrum of the residual that indicated the absence of significant modes with  $S/N$  greater than 5.2. The  $Q$  value of the radial fundamental mode is 0.032, which is in the reported range of fundamental mode for  $\delta$  Sct stars. The rectified light curve shows a peak-to-peak amplitude of about  $\sim 0.43$  mag, which is slightly more than 0.3 mag (expected for HADS stars).

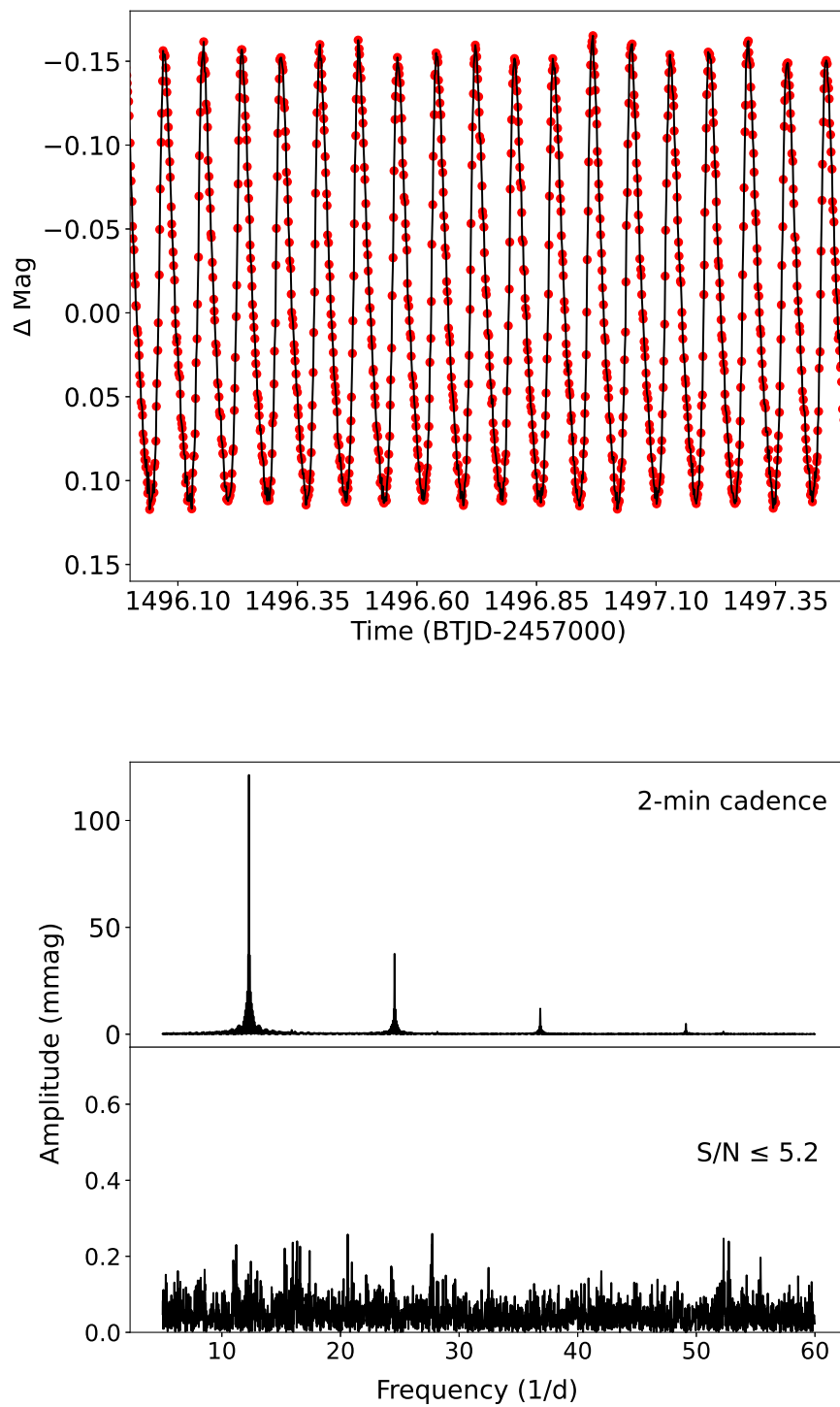
#### 4.2. TIC 130474019

Figure 4 shows the light curve (top panel), amplitude spectrum (middle panel), and amplitude spectrum of the residual (bottom panel) for TIC 130474019 (TYC 7636-1969-1). [Barceló Forteza et al. \(2020\)](#) determined the physical parameters (temperature, gravity, and frequency scaling relation) of TIC 130474019 ( $R.A. = +6^h59^m54^s.82$ ,  $DEC = -42^\circ01'15.12''$ ) using TESS observation, while [Barac et al. \(2022\)](#) introduced this star as a  $\delta$  Sct sample. This star's light curves recorded in sectors 7 and 34 include 16339 and 16850 data points, respectively. Table 3 shows the 16 frequencies, which include two radial frequencies of  $F0 = 12.28231 \text{ day}^{-1}$  (fundamental,  $P0 = 0.0814$  days) and  $F1 = 15.8872 \text{ day}^{-1}$  (first overtone) with  $Q$  values as 0.04 and 0.031 respectively. The frequency ratio ( $F0/F1$ ) is obtained to be 0.78, which indicates the independent property and validity of the fundamental and first overtone. As tabulated in Table3, we observed the harmonics frequencies ( $f_2, f_3, f_4$ ), combination frequencies ( $f_6, f_{10}, f_{11}, f_{13}$ ), and nonradial modes ( $f_7, \dots, f_9, f_{12}, f_{14}, \dots, f_{16}$ ). The peak-to-peak amplitude is about  $\sim 0.3$  mag, and the range of the frequencies might suggest TIC 130474019 is a double-mode HADS star.





**Figure 3.** The short-cadence light curve (sectors 36 and 37) of TIC 374753270 during 1.5 days (top panel), amplitude spectrum (middle panel), and amplitude spectrum of residual with S/N less than 5.2 (bottom panel).



**Figure 4.** The short-cadence light curve (sector 7) of TIC 130474019 during 1.5 days (top panel), amplitude spectrum (middle panel), and amplitude spectrum of residual with S/N less than 5.2 (bottom panel).



**Table 2.** A complete list of the 14 identified frequencies for TIC 374753270 (denoted by  $f_i$ ).

$f_i$	Frequency ( $\text{day}^{-1}$ )	Amplitude (mmag)	phase (radians/ $2\pi$ )	S/N	ID	period ratio	$Q$ value
1	7.246052±0.000002	159.91±0.03	0.50029±0.00003	1430.94	F0	-	0.032±0.004
2	14.491993±0.000004	74.91±0.03	0.31175±0.00006	1196.53	2F0	-	-
3	21.737972±0.000008	39.41±0.03	0.9745±0.0001	825.07	3F0	-	-
4	28.98394±0.00002	14.57±0.03	0.6471±0.0003	394.95	4F0	-	-
5	36.22991±0.00004	7.83±0.03	0.3280±0.0006	236.33	5F0	-	-
6	6.01456±0.00005	5.81±0.03	0.6383±0.0008	142.08	nonradial	-	-
7	43.47588±0.00007	4.46±0.03	0.961±0.001	140.41	6F0	-	-
8	50.7219±0.0001	3.14±0.03	0.264±0.001	101.92	7F0	-	-
9	57.9679±0.0001	2.45±0.03	0.023±0.002	40.28	8F0	-	-
10	12.0289±0.0002	1.34±0.03	0.939±0.003	18.88	nonradial	-	-
11	18.0437±0.0006	0.51±0.03	0.367±0.01	17.45	nonradial	-	-
12	13.2607±0.0007	0.42±0.03	0.059±0.01	15.06	nonradial	-	-
13	8.477±0.001	0.21±0.03	0.324±0.02	6.42	nonradial	-	-
14	20.506±0.001	0.18±0.03	0.902±0.02	5.33	nonradial	-	-

Note. The frequency resolution is about  $f_{res} = 0.029\text{day}^{-1}$ .

**Table 3.** A complete list of the 16 identified frequencies for TIC 130474019 (denoted by  $f_i$ ).

$f_i$	Frequency ( $\text{day}^{-1}$ )	Amplitude (mmag)	phase (radians/ $2\pi$ )	S/N	ID	period ratio	$Q$ value
1	12.28231±0.00001	121.25±0.06	0.95194±0.00008	1372.4	F0	-	0.04±0.004
2	24.56457±0.00003	37.73±0.06	0.9304±0.0002	639.01	2F0	-	-
3	36.8468±0.0001	11.96±0.06	0.7588±0.0008	279.6	3F0	-	-
4	49.1293±0.0002	4.92±0.06	0.375±0.002	106.2	4F0	-	-
5	15.8872±0.0007	1.94±0.06	0.499±0.005	18.10	F1	0.78	0.027±0.003
6	28.173±0.001	1.17±0.06	0.904±0.008	12.57	F0+F1	-	-
7	16.577±0.002	0.69±0.06	0.70±0.03	8.31	nonradial	-	-
8	16.015±0.002	0.60±0.06	0.44±0.01	7.96	nonradial	-	-
9	15.416±0.002	0.63±0.06	0.23±0.01	8.29	nonradial	-	-
10	8.672±0.002	0.47±0.06	0.02±0.02	7.18	2F0-F1	-	-
11	40.452±0.002	0.46±0.06	0.71±0.02	9.34	2F0+F1	-	-
12	28.299±0.003	0.41±0.06	0.99±0.02	8.24	nonradial	-	-
13	52.737±0.003	0.34±0.06	0.09±0.02	8.31	3F0+F1	-	-
14	15.973±0.003	0.25±0.06	0.90±0.03	5.67	nonradial	-	-
15	20.611±0.003	0.23±0.06	0.62±0.03	5.44	nonradial	-	-
16	27.699±0.003	0.22±0.06	0.43±0.03	5.23	nonradial	-	-

Note. The frequency resolution is about  $f_{res} = 0.061\text{day}^{-1}$ .

#### 4.3. TIC 148357344

Figure 5 displays the light curve (top panel), amplitude spectrum (middle panel), and amplitude spectrum of the residual (bottom panel) for TIC 148357344 (TYC 5968-1693-1). TIC 148357344 ( $R.A. = +07^h05^m28^s.9$ ,  $DEC = -17^\circ05'16.75''$ ) was first identified as a variable star by [Heinze et al. \(2018\)](#), then it was introduced as  $\delta$  Sct by [Barac et al. \(2022\)](#). TIC 148357344 was observed only in sector 7 (short-cadence) with a duration of 27 days and consisting of 16056 data points. We identified 12 frequencies for this star (Table 4), which includes three radial frequencies F0 =  $8.43\text{ day}^{-1}$  ( $P0 = 0.119$  days), F1 =  $11.09951$

**Table 4.** A complete list of the 12 identified frequencies for TIC 148357344 (denoted by  $f_i$ ).

$f_i$	Frequency ( $\text{day}^{-1}$ )	Amplitude (mmag)	phase (radians/ $2\pi$ )	S/N	ID	period ratio	$Q$ value
1	11.09951±0.00001	151.003±0.08	0.96259 ±0.00009	1948.012	F1	0.76	0.023±0.003
2	22.19904±0.00003	55.44±0.08	0.3230±0.0002	942.301	2F1	-	-
3	33.29853±0.00009	19.09±0.08	0.6087±0.0002	334.345	3F1	-	-
4	44.3980±0.0001	10.92±0.08	0.8494±0.0007	198.396	4F1	-	-
5	55.4977±0.0006	6.01±0.08	0.483±0.001	134.900	5F1	-	-
6	13.835±0.001	2.93±0.08	0.592±0.004	55.0831	F2	0.61	0.018±0.002
7	24.935±0.001	1.85±0.08	0.426±0.007	34.443	F1+F2	-	-
8	47.132±0.003	0.56±0.08	0.67±0.01	11.070	3F1+F2	-	-
9	8.43±0.003	0.51±0.08	0.98±0.02	12.999	F0	-	0.028±0.004
10	58.233±0.003	0.41±0.08	0.22±0.02	11.216	4F1+F2	-	-
11	30.559±0.004	0.39±0.08	0.610±0.003	9.018	4F1-F2	-	-
12	19.463±0.004	0.38±0.08	0.717±0.003	6.32	3F1-F2	-	-

Note. The frequency resolution is about  $f_{res} = 0.061\text{day}^{-1}$ .

$\text{day}^{-1}$  and  $F2 = 13.835\text{day}^{-1}$ , as fundamental, first, and second overtones, respectively. The frequency ratios for the first ( $F0/F1$ ) and the second ( $F0/F2$ ) overtones were obtained as 0.76 and 0.61, respectively, determining the validity of our analysis along with the  $Q$  values as 0.028, 0.023, and 0.018 for fundamental, first, and second overtones, respectively. Other frequencies may be known as harmonics ( $f_2, f_3, \dots, f_5$ ) and combination frequencies ( $f_7, f_8, f_{10}, f_{11}, f_{12}$ ). It is noticeable that the first overtone's amplitude is more significant than that of the fundamental mode, probably owing to amplitude modulation mechanisms that are well known in  $\delta$  Sct stars (Bowman et al. 2016; Lv et al. 2021; Sun et al. 2021). Consequently, further studies are necessary to illuminate the driving mechanisms, including the mode-selecting processes in  $\delta$  Scts. The light curve's peak-to-peak value of about  $\sim 0.4$  mag and the range of frequencies propose that TIC 148357344 may be a triple-mode HADS.

#### 4.4. TIC 160120432

Figure 6 shows the light curve (top panel), amplitude spectrum (middle panel), and amplitude spectrum of the residual (bottom panel) for TIC 160120432 (TYC 4638-455-1). Using NSVS and ASAS-3 databases, Otero (2007) suggested TIC 160120432 ( $R.A. = +15^h35^m30^s.40$ ,  $DEC = +85^\circ37'38.94''$ ) as a HADS star. We applied frequency analysis for combined sectors (19 and 20), individual sectors (14, 40, and 47), and combined sectors (52 and 53). We pick up the significant frequencies ( $S/N > 5.2$  and frequency resolution greater than  $0.028\text{day}^{-1}$  and  $0.061\text{day}^{-1}$  for combined and individual sectors, respectively). In Table 5, we found 25 frequencies for TIC 160120432, which include two radial frequencies  $F0 = 10.350856\text{day}^{-1}$  ( $P0 = 0.0966$  days) and  $F1 = 13.612\text{day}^{-1}$ , with  $Q$  values as 0.031 and 0.023, respectively. As shown in Table 5, we specified the harmonic frequencies ( $f_2, f_3, \dots, f_5$ ), combination frequencies ( $f_7, f_{11}, f_{12}, f_{14}$ ), and nonradial modes ( $f_6, f_8, f_9, f_{13}, f_{15}, \dots, f_{25}$ ). The light curve's peak-to-peak value is about  $\sim 0.33$  mag. The frequencies of TIC 160120432 are ranging from 9 to  $51\text{day}^{-1}$ . The frequency ratio ( $F0/F1$ ) is 0.76, and the  $Q$  values were calculated as 0.031 and 0.024 for the fundamental and first overtone, respectively. These four findings strongly verified the HADS property for TIC 160120432 as a new double-mode HADS star.

#### 4.5. TIC 278119167

Figure 7 represents the light curve (top panel), amplitude spectrum (middle panel), and amplitude spectrum of the residual (bottom panel) for TIC 278119167 (TYC 1578-1754-1). Heinze et al. (2018) categorized TIC 278119167 ( $R.A. = 18^h38^m50^s.36$ ,  $DEC = +19^\circ07'44.61''$ ) as a pulsating variable component of a contact/overcontact binary system using a probabilistic machine-learning algorithm. Our investigation indicates that TIC 278119167 is triple-mode HADS. We analyzed the light curves for two individual sectors, 40 and 53, with a duration of 28.1 and 24.98 days, respectively. Interestingly, the set of significant frequencies for the light curve of both sections is approximately the same. We identified nine frequencies constructing the star's light curve (Table 6), which includes three radial frequencies  $F0 = 9.579\text{day}^{-1}$  ( $P0 = 0.105$  days),  $F1 = 12.58960\text{day}^{-1}$  and  $F2 = 15.671\text{day}^{-1}$ , with  $Q$  values as 0.031, 0.023, and 0.018 respectively. Other frequencies may be represented as harmonics ( $f_2, f_3, f_4, f_9$ ) and combination frequencies ( $f_6, f_7$ ). Again, in this star, the amplitude modulation phenomenon is probable due to the first overtone's amplitude being more significant than the fundamental frequency's amplitude (Bowman et al. 2016; Lv et al. 2021;

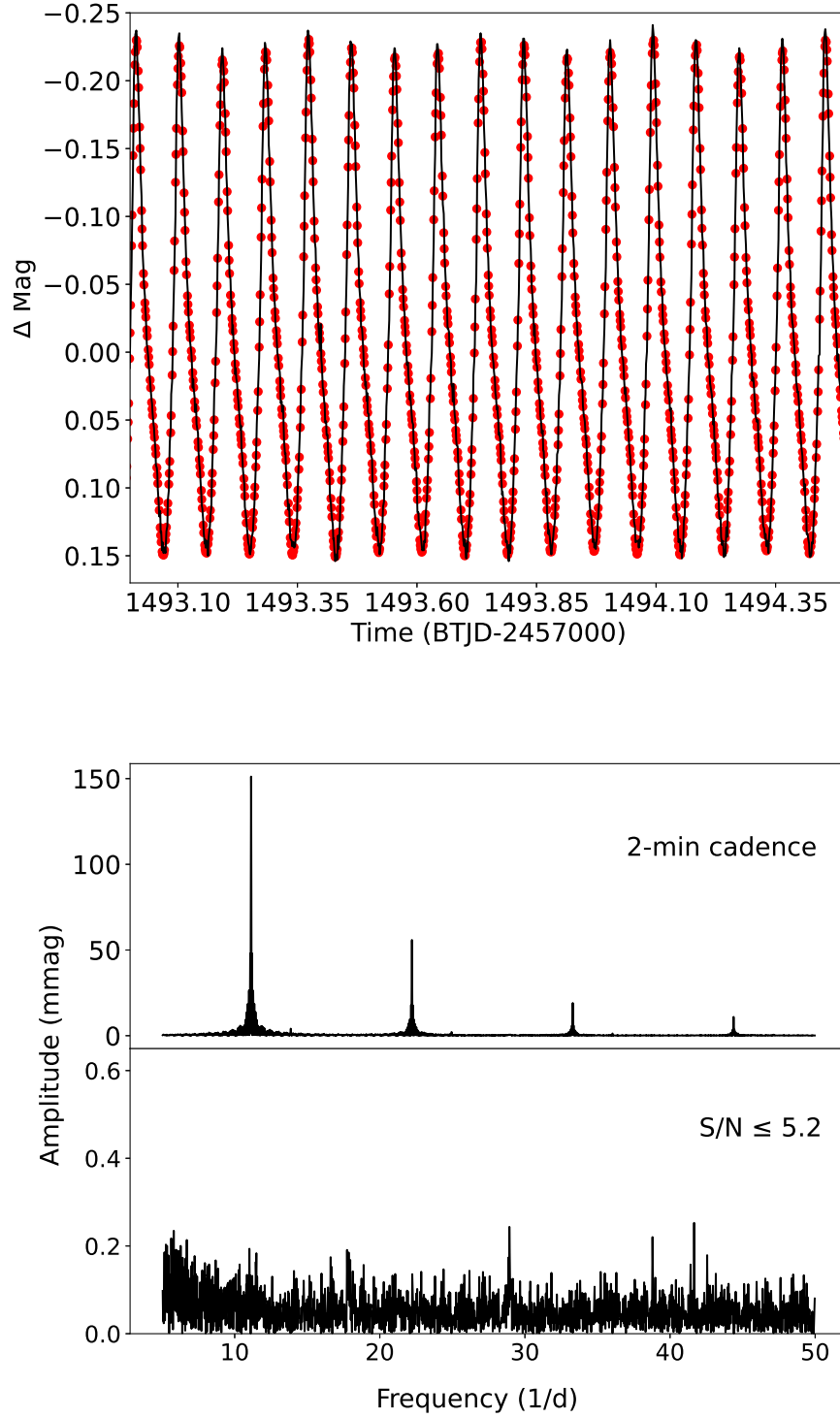


**Figure 5.** The short-cadence light curve of TIC 148357344 during 1.5 days (top panel), amplitude spectrum (middle panel), and amplitude spectrum of residual with S/N less than 5.2 (bottom panel).

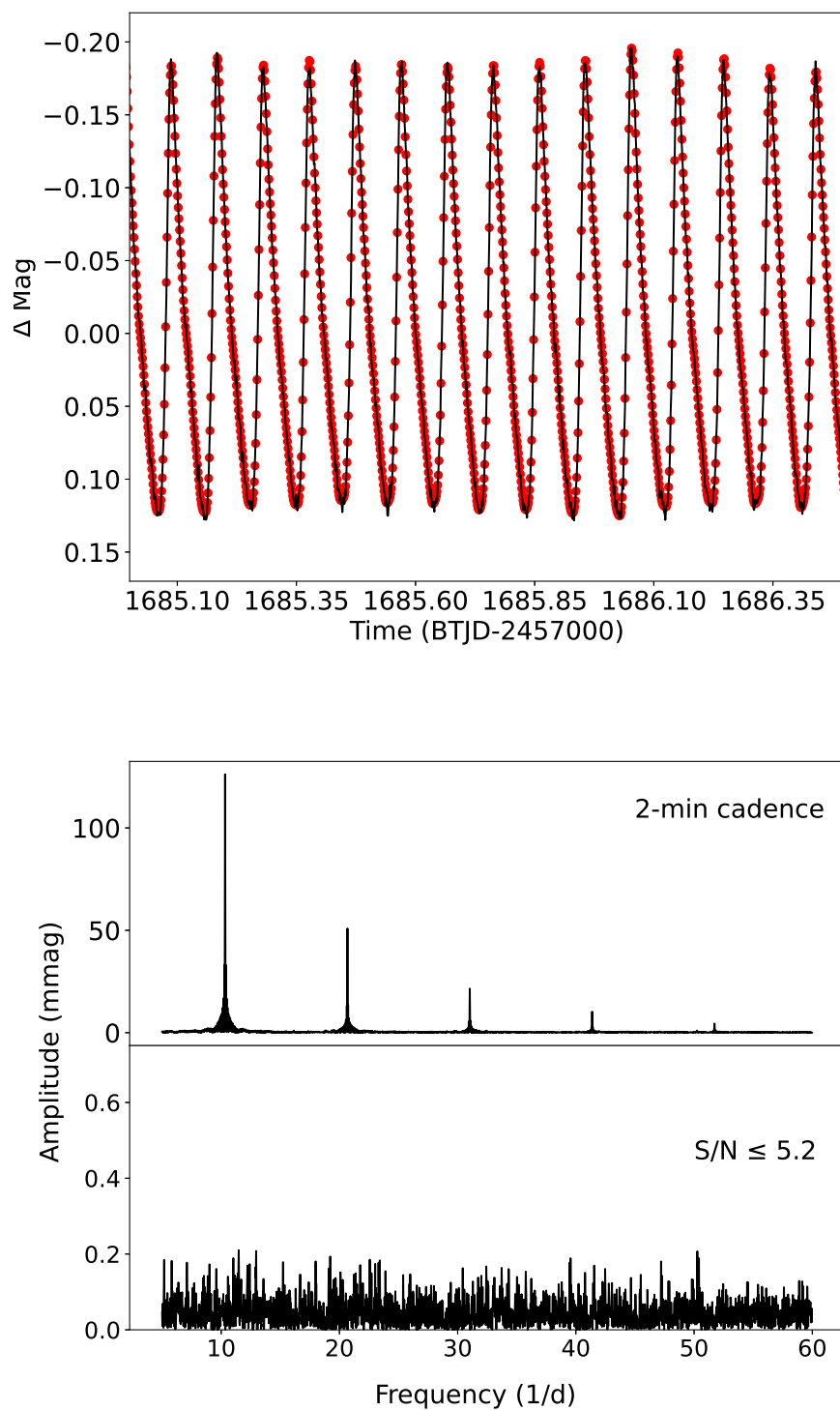


**Figure 6.** The short-cadence light curve (sector 14) of TIC 160120432 during 1.5 days (top panel), amplitude spectrum (middle panel), and amplitude spectrum of residual with S/N less than 5.2 (bottom panel).

**Table 5.** A complete list of the 25 identified frequencies for TIC 160120432 (denoted by  $f_i$ ).

$f_i$	Frequency ( $\text{day}^{-1}$ )	Amplitude (mmag)	phase (radians/ $2\pi$ )	S/N	ID	period ratio	$Q$ value
1	10.350856±0.000003	126.46±0.05	0.213±0.00006	899.46	F0	-	0.031±0.00323
2	20.701511±0.000007	50.991±0.05	0.400±0.0001	424.95	2F0	-	-
3	31.05230±0.00001	21.50±0.05	0.394±0.0003	245.05	3F0	-	-
4	41.40302±0.00003	10.378±0.05	0.710±0.0008	168.428	4F0	-	-
5	51.75381±0.00008	4.86±0.05	0.051±0.001	102.31	5F0	-	-
6	9.6819±0.0006	1.167±0.05	0.503±0.007	10.71	nonradial	-	-
7	19.5715±0.0007	0.956±0.05	0.833±0.008	11.01	6F1-6F0	-	-
8	16.1607±0.0009	1.069±0.05	0.641±0.007	15.85	nonradial	-	-
9	18.8482±0.0001	0.912±0.05	0.754±0.002	9.24	nonradial	-	-
10	13.612±0.001	0.219±0.05	0.062±0.03	8.880	F1	0.76	0.023±0.003
11	29.9194±0.0008	0.625±0.05	0.249±0.01	9.96	6F1-5F0	-	-
12	9.219±0.001	0.546±0.05	0.626±0.01	6.89	6F1-7F0	-	-
13	26.510±0.001	0.524±0.05	0.745±0.01	9.74	nonradial	-	-
14	40.269±0.001	0.487±0.05	0.836±0.01	7.45	6F1-4F0	-	-
15	19.6427±0.0009	0.555±0.05	0.416±0.01	8.24	nonradial	-	-
16	40.0626±0.0009	0.511±0.05	0.167±0.01	9.80	nonradial	-	-
17	19.4962±0.0005	0.539±0.05	0.876±0.01	7.772	nonradial	-	-
18	30.380±0.001	0.458±0.05	0.680±0.01	7.127	nonradial	-	-
20	18.8807±0.0002	0.531±0.05	0.280±0.02	8.329	nonradial	-	-
21	29.8476±0.0006	0.57±0.05	0.002±0.02	9.66	nonradial	-	-
22	22.0570±0.0008	0.48±0.05	0.22±0.02	9.64	nonradial	-	-
23	40.336±0.001	0.35±0.05	0.74±0.02	7.47	nonradial	-	-
24	15.520±0.001	0.34±0.05	0.25±0.02	7.51	nonradial	-	-
25	9.737±0.001	0.36±0.05	0.31±0.02	6.56	nonradial	-	-

**Table 6.** A complete list of the Nine identified frequencies for TIC 278119167 (denoted by  $f_i$ ).

$f_i$	Frequency ( $\text{day}^{-1}$ )	Amplitude (mmag)	phase (radians/ $2\pi$ )	S/N	ID	period ratio	$Q$ value
1	12.58960±0.00002	176.2±0.1	0.5448±0.0002	797.74	F1	0.76	0.023±0.002
2	25.17914±0.00007	49.6±0.1	0.1273±0.0006	565.91	2F1	-	-
3	37.7685±0.0003	9.7±0.1	0.051±0.003	142.05	3F1	-	-
4	50.3583±0.0006	5.3±0.1	0.745±0.005	95.015	4F1	-	-
5	15.671±0.002	1.5±0.1	0.46±0.01	15.85	F2	0.61	0.018±0.002
6	18.746±0.002	1.4±0.1	0.19±0.02	18.098	2F2-F1	-	-
7	28.260±0.003	1.0±0.1	0.48±0.02	16.202	F1+F2	-	-
8	9.579±0.005	0.2±0.1	0.47±0.04	5.31	F0	-	0.031±0.003
9	31.323±0.005	0.7±0.1	0.64±0.08	11.72	2F2	-	-

Note. The frequency resolution is about  $f_{res} = 0.053\text{day}^{-1}$ .

Sun et al. 2021). Consequently, further studies are necessary to illuminate the driving mechanisms and mode-selecting processes, which are still not fully understood in  $\delta$  Sct stars. The rectified light curve shows a peak-to-peak amplitude of about  $\sim 0.43$  mag, which may be suggested as a new triple-mode HADS.

#### 4.6. TIC 710783

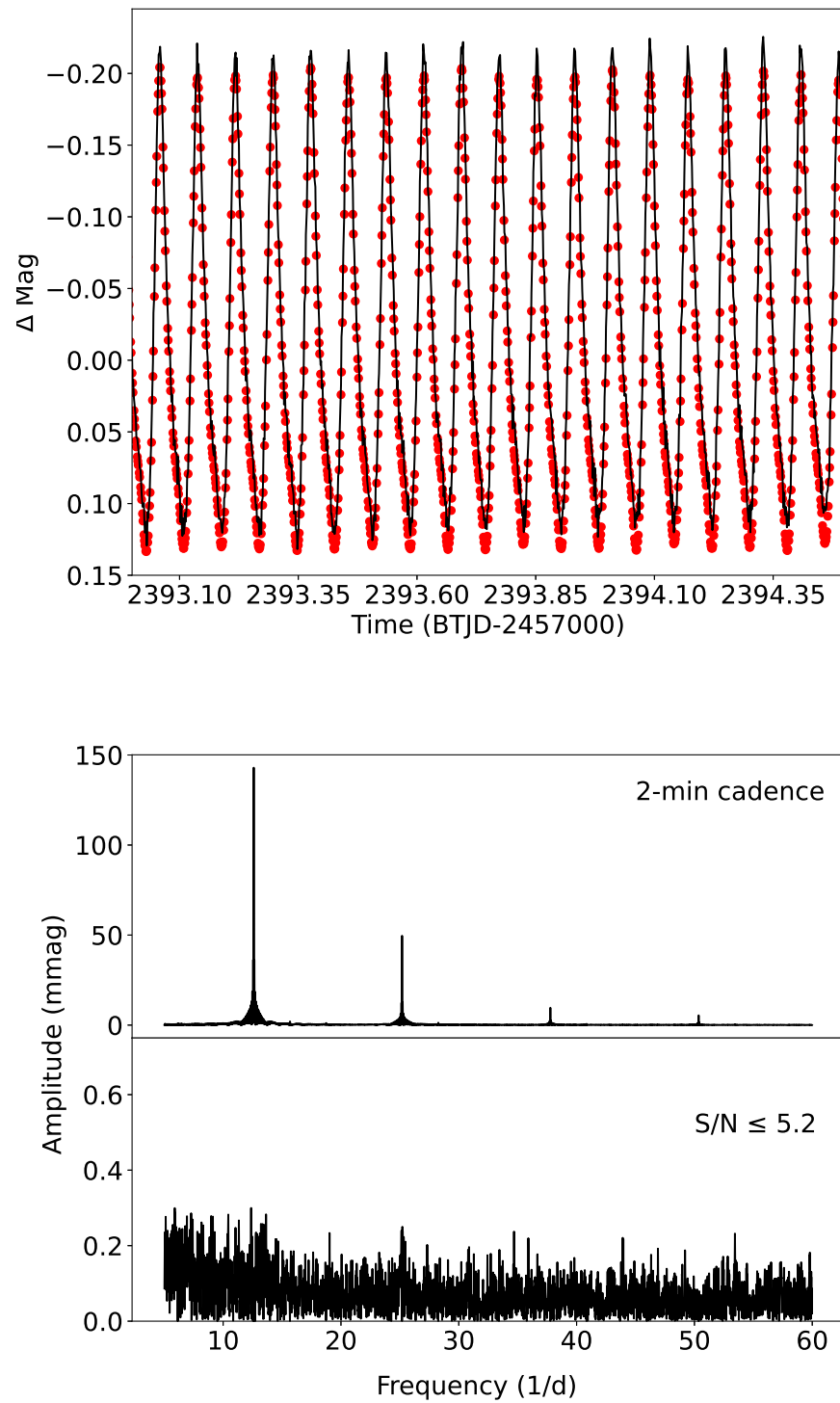


**Figure 7.** The short-cadence light curve (sector 40) of TIC 278119167 during 1.5 days (top panel), amplitude spectrum (middle panel), and amplitude spectrum of residual with S/N less than 5.2 (bottom panel).

**Table 7.** A complete list of the 11 identified frequencies for TIC 710783 (denoted by  $f_i$ ).

$f_i$	Frequency ( $\text{day}^{-1}$ )	Amplitude (mmag)	phase (radians/ $2\pi$ )	S/N	ID	period ratio	$Q$ value
1	12.74451±0.00005	164.6±0.4	0.4635±0.0003	738.43	F0	-	0.039±0.003
2	25.4890±0.0001	57.8±0.4	0.828±0.001	350.83	2F0	-	-
3	38.2334±0.0004	19.7±0.4	0.29±0.03	126.32	3F0	-	-
4	50.977±0.001	7.8±0.4	0.922±0.008	68.48	4F0	-	-
5	7.255±0.003	2.8±0.4	0.89±0.02	10.83	nonradial	-	-
6	36.277±0.003	2.7±0.4	0.18±0.02	22.87	nonradial	-	-
7	5.489±0.003	2.4±0.4	0.73±0.02	7.88	nonradial	-	-
8	32.745±0.003	2.3±0.4	0.37±0.02	18.55	nonradial	-	-
9	54.508±0.006	1.4±0.4	0.63±0.04	11.05	nonradial	-	-
10	18.231±0.008	1.0±0.4	0.74±0.06	8.35	nonradial	-	-
11	11.838±0.009	0.9±0.4	0.76±0.07	5.44	nonradial	-	-

Note. The frequency resolution is about  $f_{res} = 0.058\text{day}^{-1}$ .

**Table 8.** A complete list of the Four identified frequencies for TIC 187386415 (denoted by  $f_i$ ).

$f_i$	Frequency ( $\text{day}^{-1}$ )	Amplitude (mmag)	phase (radians/ $2\pi$ )	S/N	ID	period ratio	$Q$ value
1	14.49465±0.00003	113.8±0.1	0.5514±0.0001	473.8	F0	-	0.033±0.0045
2	28.98936±0.00009	41.0±0.1	0.8682±0.0005	333.91	2F0	-	-
3	43.4840±0.0002	15.6±0.1	0.223±0.001	196.24	3F0	-	-
4	57.9786±0.0005	7.5±0.1	0.989±0.003	93.54	4F0	-	-

Note. The frequency resolution is about  $f_{res} = 0.078\text{day}^{-1}$ .

Figure 8 represents the light curve (top panel), amplitude spectrum (middle panel), and amplitude spectrum of the residual (bottom panel) for TIC 710783 (ATO J074.1485-27.6801). The TIC 710783 ( $R.A. = 04^h56^m35^s.63$ ,  $DEC = -27^\circ40'48.56''$ ) was first recognized as a variable star by [Heinze et al. \(2018\)](#), and then its physical parameters (temperature, gravity, and frequency scaling relation) were measured by [Barceló Forteza et al. \(2020\)](#) as a  $\delta$  Sct star. We suggest that TIC 710783 shows signs of a single-mode HADS. The TESS space telescope recorded TIC 710783 during sector 5 for 25.43 days and consisting 17,023 data points. We identified 11 frequencies constructing the star's light curve (Table 7), which includes a radial frequency F0 = 12.74451  $\text{day}^{-1}$  (P0 = 0.078 days), with  $Q$  value as 0.039. We observed the harmonics frequencies ( $f_2, f_3, f_4$ ) and nonradial modes ( $f_5, f_6, \dots, f_{11}$ ). The light curve's peak-to-peak value of about  $\sim 0.47$  mag and the range of frequencies propose that TIC 710783 may be a new monomode HADS.

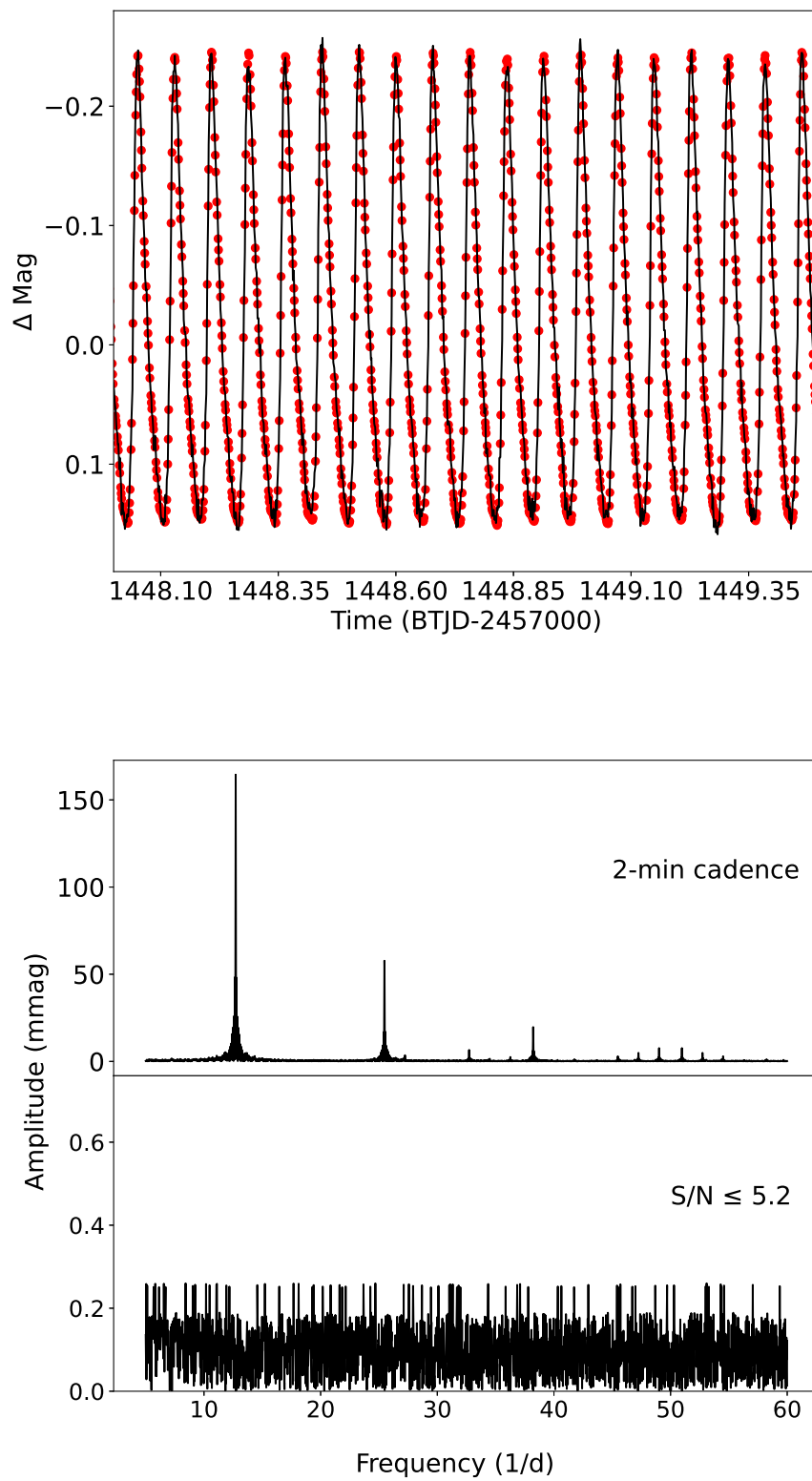
#### 4.7. TIC 187386415

Figure 9 represents the light curve (top panel), amplitude spectrum (middle panel), and amplitude spectrum of the residual (bottom panel) for TIC 187386415 (ATO J236.5561-00.4351). TIC 187386415 ( $R.A. = 15^h46^m13^s.48$ ,  $DEC = -00^\circ26'06.34''$ ) was classified by [Hey et al. \(2021\)](#) as a variable star. This study shows that TIC 187386415 is a single-mode HADS. We analyzed this star for sector 51 with a duration of 19.13 days and consisting of 6775 data points. We identified four frequencies constructing the star's light curve (Table 8), which includes a radial frequency F0 = 14.49465  $\text{day}^{-1}$  (P0 = 0.069 days), with  $Q$  value as 0.033. Other frequencies may be introduced as harmonic frequencies ( $f_2, f_3, f_4$ ). The peak-to-peak amplitude ( $\sim 0.31$  mag) and the frequencies' range propose that TIC 187386415 may be a new monomode HADS star.

#### 4.8. Asteroseismical parameters vs. physical quantities

Using Equation (3), we obtained the absolute magnitudes and their errors (applying errors of apparent magnitudes and parallaxes) for seven HADS stars. We calculated the period (P0) of each star using the fundamental frequency (Tables 2-8). Figure 10 (left





**Figure 8.** The short-cadence light curve of TIC 710783 during 1.5 days (top panel), amplitude spectrum (middle panel), and amplitude spectrum of residual with S/N less than 5.2 (bottom panel).

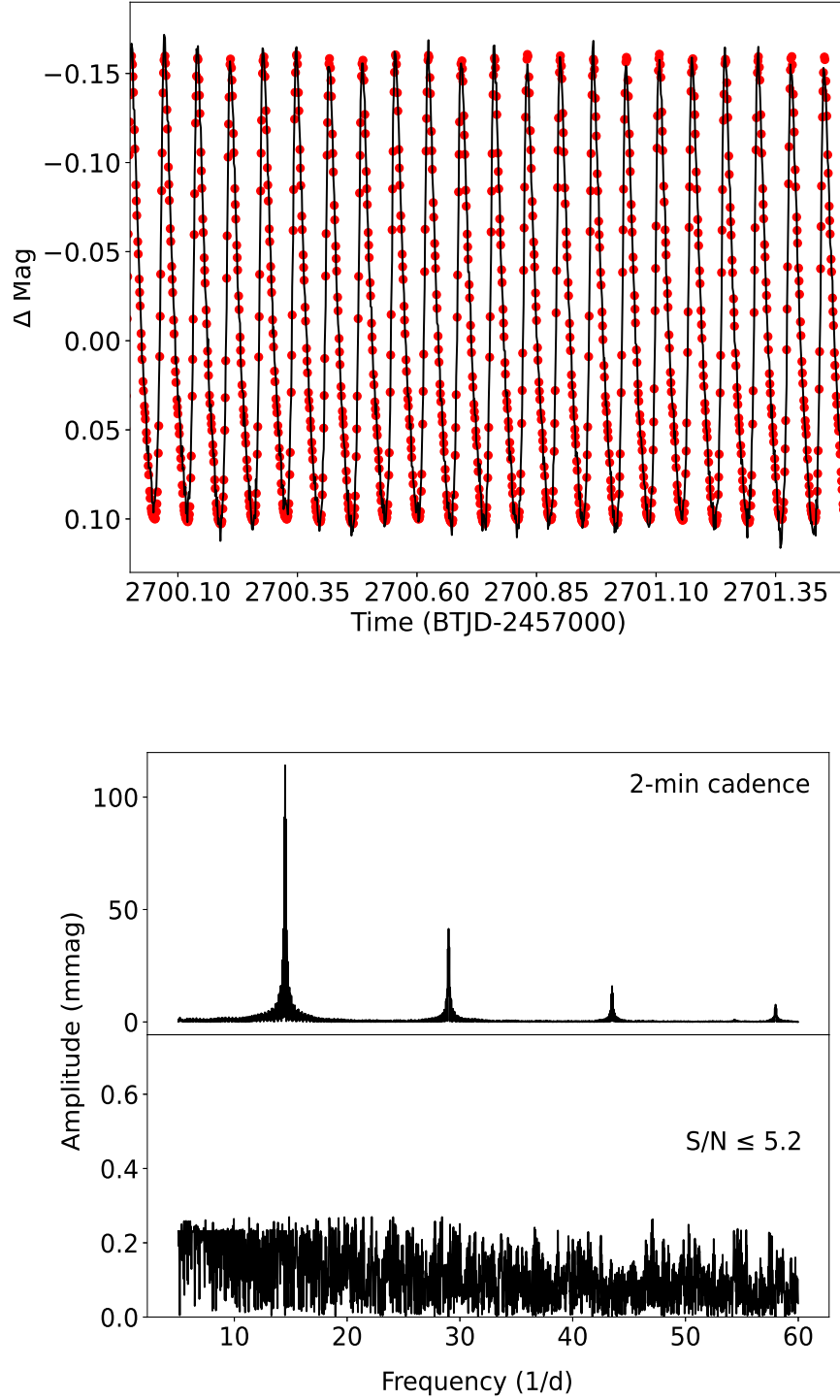


**Figure 9.** The short-cadence light curve of TIC 187386415 during 1.5 days (top panel), amplitude spectrum (middle panel), and amplitude spectrum of residual with S/N less than 5.2 (bottom panel).

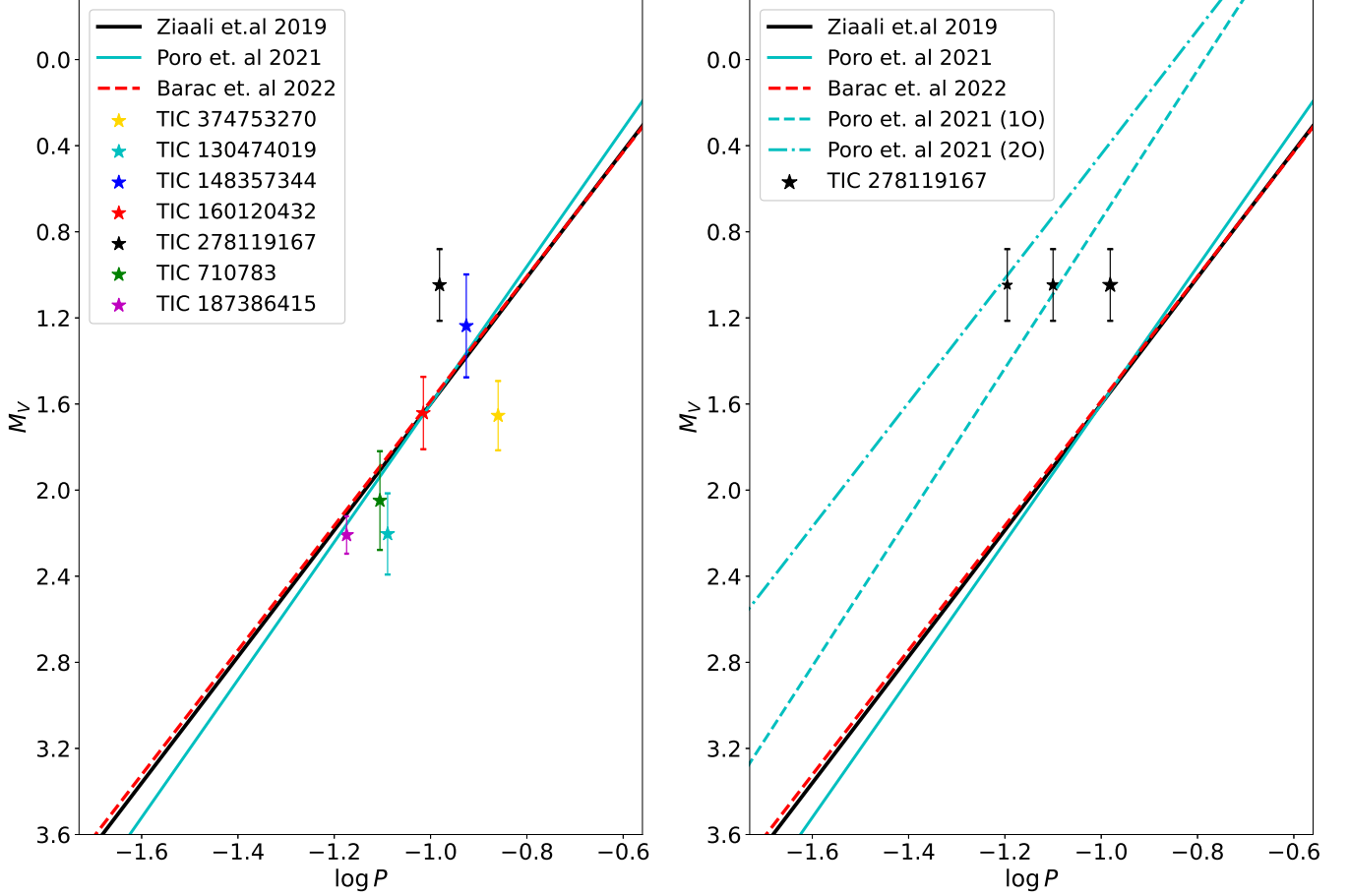


**Figure 10.** (Left panel) The period-luminosity (PL) diagram of our HADS stars (colored star markers). The solid black line shows the relation from Ziaali et al. (2019) (see Equation 5). The diagonal dashed red line shows the relation from Barac et al. (2022) (see Equation 6). The cyan dashed–dotted line shows the relation from Poro et al. (2021) (see Equation 7). The error bars indicate the errors for absolute magnitudes. (Right panel) The PL relation of TIC 278119167 for the first (cyan dashed line) and second (cyan dotted line) overtones. While the fundamental mode (the largest star marker) slightly deviates from fundamental lines, the first (the middle-sized star marker) and second (the smallest star marker) overtones are entirely consistent with their PL relations.

panel) shows the PL relation for our HADS stars (colored star markers), the PL relation of Equation (5) (solid black), Equation (6) (red dashed line), and Equation (7) (cyan dashed–dotted line). For stars TIC 374753270 and TIC 130474019, the fundamental period and absolute magnitude agreed with Barac et al. (2022). As shown in Figure 10, all seven cases satisfy the PL relation for  $\delta$  Sct stars. that indicates the validity of our frequency analysis.

Figure 10 (right panel) examines the first and second overtone periods of TIC 278119167 by PL relations for the first (dashed line) and second (dashed–dotted line) overtones. The PL relation for the first and second overtones was obtained by Poro et al. (2021). While the TIC 278119167 star’s fundamental period (shown as the largest star marker) slightly deviates from the fundamental PL relation, the first overtone period (the middle-sized star marker) and the second overtone period (the smallest star marker) entirely agree with the first and second overtone PL relations. This implies the validity of the identified fundamental frequency for TIC 278119167.

Stellar metallicity is the abundance of elements heavier than hydrogen and helium. However, in astrophysics, it is often written as the ratio of iron to hydrogen relative to the solar value ( $[\text{Fe}/\text{H}]$ ; Kotoneva et al. (2002); Chruslinska & Nelemans (2019)). Netzel & Smolec (2022) obtained the  $[\text{Fe}/\text{H}]$  for 176 HADS stars by applying the MESA, Warsaw code, and optimization procedure. These 176 HADS stars are mostly multimode (P0, P1, P2,...) cases. The metallicity distribution for these 176 HADS stars ranges from -0.2 to 0.5 dex, which may be slightly related to the dispersion of period ratio (P1/P0 and P2/P0). Lv et al. (2023) obtained a linear relation for period ratios (P1/P0 and P2/P0) and fundamental period P0 (Figures 10 and 11 therein).

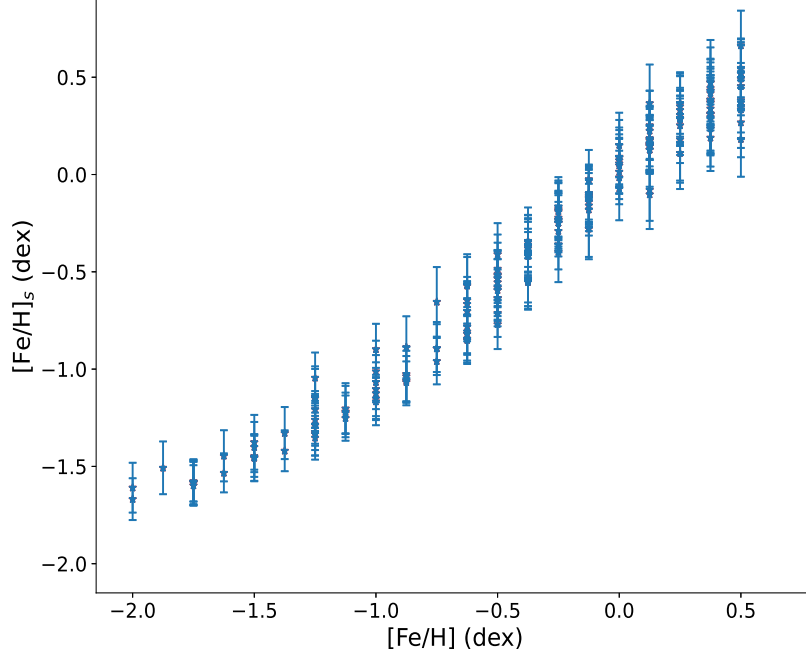


**Figure 11.** The scaling metallicity  $[\text{Fe}/\text{H}]_s$  (Equation 8) versus the metallicity  $[\text{Fe}/\text{H}]$  for 176 HADS stars (Netzel & Smolec 2022).

Therefore, we may consider the P1 and P2 as a function of P0 that allows us to investigate the scaling relation between metallicity, physical parameters, and fundamental period (P0).

Using the mass ( $M$ ), luminosity ( $L$ ), fundamental period (P0), and the effective temperature ( $T_{\text{eff}}$ ) of these 176 HADS stars, we determined the following scaling relation for  $[\text{Fe}/\text{H}]$  as

$$[\text{Fe}/\text{H}]_s = \log_{10} \left( \left( \frac{M}{M_{\odot}} \right)^{7.95 \pm 0.15} \left( \frac{L}{L_{\odot}} \right)^{-1.83 \pm 0.11} \left( \frac{\text{P0}(\text{day})}{0.064} \right)^{0.79 \pm 0.14} \left( \frac{T_{\text{eff}}}{\text{K}} \right)^{0.047 \pm 0.02} \right), \quad (8)$$

where  $[\text{Fe}/\text{H}]_s$  is the scaling metallicity obtained by an optimization procedure for 176 HADS stars. The plus/minus values indicate the standard error of the power indexes in the model that obtained by the optimization algorithm. Figure 11 shows the comparison of  $[\text{Fe}/\text{H}]$  and scaling  $[\text{Fe}/\text{H}]_s$  (Equation 8) for HADS stars. Using Equation (8), we obtained the  $[\text{Fe}/\text{H}]_s$  of our seven newly identified HADS stars. We estimated the metallicity ranging from -0.62 to 0.37 dex (Table 9) for these seven HADS stars. Equation (8) is the scaling relation for the metallicity of multimode HADS, while three of our HADS (TIC 374753270, TIC 710783, and TIC 187386415) are the single-modes stars. Therefore, estimating the metallicity of three targets using Equation (8) may contain some uncertainty.

The four HADS stars (TIC 374753270, TIC 148357344, TIC 160120432, and TIC 278119167) show lower iron abundance than the Sun, while the rest of the three HADS (TIC 130474019, TIC 710783, and TIC 187386415) demonstrate positive  $[\text{Fe}/\text{H}]$ . The metallicities of these seven HADS stars are more significant than -0.5 dex, indicating metal-rich behavior (McNamara 2011). The metal-rich behavior is an essential characteristic of the evolved old stars.

## 5. CONCLUSION

To probe the new HADS stars from recent TESS observations of  $\delta$  Sct stars, we recognized seven new targets, namely TIC 374753270, TIC 13047401, TIC 148357344, TIC 160120432, TIC 278119167, TIC 71083, and TIC 187386415, which show the peak-to-peak amplitude slightly more significant than 0.3 mag in their light curves. Using Equation (3) and the Gaia DR3 parallaxes, the  $V$ -band absolute magnitude was calculated for these seven stars. Applying the TESS effective temperatures from Stassun et al. (2018) and the obtained absolute magnitudes, these seven HADS stars were located in the H-R diagram. They lie in the  $\delta$  Sct stars' stability strip of the H-R diagram (Figure 2) close to the cooler boundary.

The HADS stars were expected to show a simple amplitude spectrum, including one to a few large amplitudes. The period ratios,  $Q$  values, and PL relation between the fundamental radial frequency and luminosity were used to show the validity of mode information for these seven stars. We applied the frequency analysis to obtain information on the significant frequencies of these

**Table 9.** TIC number, mass ( $M/M_{\odot}$ ), radius ( $R/R_{\odot}$ ), surface gravity ( $\log g$ ), effective temperature ( $T_{\text{eff}}$ ), absolute  $V$ -band magnitude ( $M_V$ ), and metallicity ( $[\text{Fe}/\text{H}]_s$ ) for seven HADS stars.

TIC number	$M/M_{\odot}$	$R/R_{\odot}$	$\log g$ ( $\text{cm/s}^2$ )	$T_{\text{eff}}$ (K)	$M_V$	$[\text{Fe}/\text{H}]_s$ (dex)
374753270	$1.60 \pm 0.20$	$3.04 \pm 0.22$	$3.67 \pm 0.11$	$7166 \pm 304.2$	$1.61 \pm 0.16$	$-0.451 \pm 0.161$
130474019	$1.76 \pm 0.21$	$1.93 \pm 0.09$	$4.11 \pm 0.10$	$7573 \pm 197.5$	$2.20 \pm 0.18$	$0.243 \pm 0.135$
148357344	$1.61 \pm 0.21$	$2.99 \pm 0.22$	$3.69 \pm 0.06$	$7183 \pm 270$	$1.51 \pm 0.23$	$-0.465 \pm 0.160$
160120432	$1.59 \pm 0.19$	$2.51 \pm 0.13$	$3.84 \pm 0.08$	$7138 \pm 153.8$	$1.61 \pm 0.16$	$-0.266 \pm 0.143$
278119167	$1.68 \pm 0.2$	$2.68 \pm 0.13$	$3.80 \pm 0.08$	$7369 \pm 185.1$	$1.05 \pm 0.16$	$-0.271 \pm 0.154$
710783	$1.77 \pm 0.23$	$1.92 \pm 0.09$	$4.11 \pm 0.07$	$7604 \pm 150.9$	$2.04 \pm 0.22$	$0.237 \pm 0.135$
187386415	$1.67 \pm 0.20$	$1.93 \pm 0.16$	$4.08 \pm 0.08$	$7340 \pm 97.2$	$2.20 \pm 0.08$	$0.098 \pm 0.130$

Note. These physical parameters (mass, radius, surface gravity, and effective temperature) of seven targets are given by Stassun et al. (2018). Using Equations (3, 8), the absolute  $V$ -band magnitude ( $M_V$ ) and metallicity ( $[\text{Fe}/\text{H}]_s$ ) were calculated.

stars. The significant frequencies followed an S/N greater than 5.2. Our analyses show that the HADS stars were categorized into single modes (TIC 374753270, TIC 710783, and TIC 187386415), double modes (TIC 130474019 and TIC 160120432), and triple modes (TIC 148357344 and TIC 278119167). We determined the variety of harmonic and combination frequencies in the amplitude spectrum of targets (Tables 2-8) as well as nonradial oscillation frequencies for most of our targets. We derived a scaling relation using 176 HADS stars from Netzel & Smolec (2022) between metallicity ( $[\text{Fe}/\text{H}]$ ) and physical parameters (mass ( $M$ ), luminosity ( $L$ ), and the effective temperature ( $T_{\text{eff}}$ )) and fundamental period ( $P_0$ ). Using Equation (8), we estimated the metallicity of the seven HADS stars. The metallicity of all seven stars is greater than -0.62 dex, as expected of the HADS stars.

## 6. ACKNOWLEDGMENTS

This paper includes data collected by the TESS mission, which are publicly available from the Mikulski Archive for Space Telescopes (MAST). Funding for the TESS mission is provided by the NASA Explorer Program. Funding for the TESS Asteroseismic Science Operations Centre is provided by the Danish National Research Foundation (grant agreement No.: DNRFF106), ESA PRODEX (PEA 4000119301), and Stellar Astrophysics Centre (SAC) at Aarhus University. We would like to thank the Gaia team for providing accurate data from the European Space Agency (ESA) mission Gaia, processed by the Gaia Data Processing and Analysis Consortium (DPAC). Funding for the DPAC has been provided by national institutions, in particular, the institutions participating in the Gaia Multilateral Agreement. This work has been supported by the Iran National Science Foundation (INSF) under grant No. 4002562. E.Z. expresses gratitude for that. Also, E.Z. acknowledges financial support from project PID2019-107061GB-C63 from the ‘Programas Estatales de Generación de Conocimiento y Fortalecimiento Científico y Tecnológico del Sistema de I+D+i y de I+D+i Orientada a los Retos de la Sociedad’ and from the grant CEX2021-001131-S funded by MCIN/AEI/10.13039/501100011033.

## REFERENCES

- 1997ESA. 1997, ESA Special Publication, Vol. 1200, The HIPPARCOS and TYCHO catalogues. Astrometric and photometric star catalogues derived from the ESA HIPPARCOS Space Astrometry Mission
- Aerts, C., Christensen-Dalsgaard, J., & Kurtz, D. W. 2010, Asteroseismology (Springer Netherlands), doi: [10.1007/978-1-4020-5803-5](https://doi.org/10.1007/978-1-4020-5803-5)
- Aguirre, V. S., Davies, G. R., Basu, S., et al. 2015, Monthly Notices of the Royal Astronomical Society, 452, 2127, doi: [10.1093/mnras/stv1388](https://doi.org/10.1093/mnras/stv1388)
- Antoci, V. 2013, Proceedings of the International Astronomical Union, 9, 333–340, doi: [10.1017/s1743921313014543](https://doi.org/10.1017/s1743921313014543)
- Antoci, V., Handler, G., Campante, T. L., et al. 2011, Nature, 477, 570, doi: [10.1038/nature10389](https://doi.org/10.1038/nature10389)
- Antoci, V., Cunha, M. S., Bowman, D. M., et al. 2019, MNRAS, 490, 4040, doi: [10.1093/mnras/stz2787](https://doi.org/10.1093/mnras/stz2787)
- Baker, N., & Kippenhahn, R. 1962, ZA, 54, 114
- Balmforth, N. J., & Gough, D. O. 1990, ApJ, 362, 256, doi: [10.1086/169262](https://doi.org/10.1086/169262)
- Barac, N., Bedding, T. R., Murphy, S. J., & Hey, D. R. 2022, MNRAS, 516, 2080, doi: [10.1093/mnras/stac2132](https://doi.org/10.1093/mnras/stac2132)
- Baran, A. S., Koen, C., & Pkrzyżwka, B. 2015, MNRAS, 448, L16, doi: [10.1093/mnras/lu194](https://doi.org/10.1093/mnras/lu194)

- Barceló Forteza, S., Moya, A., Barrado, D., et al. 2020, *A&A*, 638, A59, doi: [10.1051/0004-6361/201937262](https://doi.org/10.1051/0004-6361/201937262)
- Barclay, T., Pepper, J., & Quintana, E. V. 2018, *ApJS*, 239, 2, doi: [10.3847/1538-4365/aae3e9](https://doi.org/10.3847/1538-4365/aae3e9)
- Bedding, T. R., Murphy, S. J., Hey, D. R., et al. 2020, *Nature*, 581, 147, doi: [10.1038/s41586-020-2226-8](https://doi.org/10.1038/s41586-020-2226-8)
- Bono, G., Caputo, F., Cassisi, S., et al. 1997, *ApJ*, 477, 346, doi: [10.1086/303710](https://doi.org/10.1086/303710)
- Bowman, D. M. 2017, *Amplitude Modulation of Pulsation Modes in Delta Scuti Stars* (Springer), doi: [10.1007/978-3-319-66649-5](https://doi.org/10.1007/978-3-319-66649-5)
- Bowman, D. M., Kurtz, D. W., Breger, M., Murphy, S. J., & Holdsworth, D. L. 2016, *MNRAS*, 460, 1970, doi: [10.1093/mnras/stw1153](https://doi.org/10.1093/mnras/stw1153)
- Bowman, D. M., & Michielsen, M. 2021, *Astronomy & Astrophysics*, 656, A158, doi: [10.1051/0004-6361/202141726](https://doi.org/10.1051/0004-6361/202141726)
- Breger, M. 1979, *Publications of the Astronomical Society of the Pacific*, 91, 5, doi: [10.1086/130433](https://doi.org/10.1086/130433)
- Breger, M. 1990, in *Astronomical Society of the Pacific Conference Series*, Vol. 11, *Confrontation Between Stellar Pulsation and Evolution*, ed. C. Cacciari & G. Clementini, 263–273
- Breger, M. 2000a, in *Astronomical Society of the Pacific Conference Series*, Vol. 210, *Delta Scuti and Related Stars*, ed. M. Breger & M. Montgomery, 3
- Breger, M. 2000b, *MNRAS*, 313, 129, doi: [10.1046/j.1365-8711.2000.03185.x](https://doi.org/10.1046/j.1365-8711.2000.03185.x)
- Breger, M., & Bregman, J. N. 1975, *ApJ*, 200, 343, doi: [10.1086/153794](https://doi.org/10.1086/153794)
- Breger, M., Balona, L., Lenz, P., et al. 2011, *Monthly Notices of the Royal Astronomical Society*, 414, 1721, doi: [10.1111/j.1365-2966.2011.18508.x](https://doi.org/10.1111/j.1365-2966.2011.18508.x)
- Chang, S. W., Protopapas, P., Kim, D. W., & Byun, Y. I. 2013, *AJ*, 145, 132, doi: [10.1088/0004-6256/145/5/132](https://doi.org/10.1088/0004-6256/145/5/132)
- Chruslinska, M., & Nelemans, G. 2019, *Monthly Notices of the Royal Astronomical Society*, 488, 5300, doi: [10.1093/mnras/stz2057](https://doi.org/10.1093/mnras/stz2057)
- Dékány, I., & Grebel, E. K. 2022, *ApJS*, 261, 33, doi: [10.3847/1538-4365/ac74ba](https://doi.org/10.3847/1538-4365/ac74ba)
- Dupret, M. A., Grigahcène, A., Garrido, R., Gabriel, M., & Scuflaire, R. 2005, *A&A*, 435, 927, doi: [10.1051/0004-6361:20041817](https://doi.org/10.1051/0004-6361:20041817)
- Gilliland, R. L., Brown, T. M., Christensen-Dalsgaard, J., et al. 2010, *PASP*, 122, 131, doi: [10.1086/650399](https://doi.org/10.1086/650399)
- Green, G. M., Schlafly, E. F., Finkbeiner, D., et al. 2018, *MNRAS*, 478, 651, doi: [10.1093/mnras/sty1008](https://doi.org/10.1093/mnras/sty1008)
- Guzik, J. A. 2021, *Frontiers in Astronomy and Space Sciences*, 8, 55, doi: [10.3389/fspas.2021.653558](https://doi.org/10.3389/fspas.2021.653558)
- Handler, G. 2009, in *American Institute of Physics Conference Series*, Vol. 1170, *Stellar Pulsation: Challenges for Theory and Observation*, ed. J. A. Guzik & P. A. Bradley, 403–409, doi: [10.1063/1.3246528](https://doi.org/10.1063/1.3246528)
- Hasanzadeh, A., Safari, H., & Ghasemi, H. 2021, *MNRAS*, 505, 1476, doi: [10.1093/mnras/stab1411](https://doi.org/10.1093/mnras/stab1411)
- Heinze, A. N., Tonry, J. L., Denneau, L., et al. 2018, *AJ*, 156, 241, doi: [10.3847/1538-3881/aae47f](https://doi.org/10.3847/1538-3881/aae47f)
- Hey, D. R., Montet, B. T., Pope, B. J. S., Murphy, S. J., & Bedding, T. R. 2021, *AJ*, 162, 204, doi: [10.3847/1538-3881/ac1b9b](https://doi.org/10.3847/1538-3881/ac1b9b)
- Høg, E., Fabricius, C., Makarov, V. V., et al. 2000, *A&A*, 355, L27
- Holdsworth, D. L., Cunha, M. S., Lares-Martiz, M., et al. 2024, *MNRAS*, 527, 9548, doi: [10.1093/mnras/stad3800](https://doi.org/10.1093/mnras/stad3800)
- Houdek, G., Balmforth, N. J., Christensen-Dalsgaard, J., & Gough, D. O. 1999, *A&A*, 351, 582, doi: [10.48550/astro-ph/9909107](https://doi.org/10.48550/astro-ph/9909107)
- Jayasinghe, T., Stanek, K. Z., Kochanek, C. S., et al. 2020, *MNRAS*, 493, 4186, doi: [10.1093/mnras/staa499](https://doi.org/10.1093/mnras/staa499)
- Jenkins, J. M., Twicken, J. D., McCauliff, S., et al. 2016, in *Society of Photo-Optical Instrumentation Engineers (SPIE) Conference Series*, Vol. 9913, *Software and Cyberinfrastructure for Astronomy IV*, ed. G. Chiozzi & J. C. Guzman, 99133E, doi: [10.1117/12.2233418](https://doi.org/10.1117/12.2233418)
- Kotoneva, E., Flynn, C., & Jimenez, R. 2002, *Monthly Notices of the Royal Astronomical Society*, 335, 1147, doi: [10.1046/j.1365-8711.2002.05690.x](https://doi.org/10.1046/j.1365-8711.2002.05690.x)
- Leavitt, H. S., & Pickering, E. C. 1912, *Harvard College Observatory Circular*, 173, 1
- Lenz, P., & Breger, M. 2005, *Communications in Asteroseismology*, 146, 53, doi: [10.1553/cia146s53](https://doi.org/10.1553/cia146s53)
- Li, X.-Y., Huang, Y., Liu, G.-C., Beers, T. C., & Zhang, H.-W. 2023, *The Astrophysical Journal*, 944, 88, doi: [10.3847/1538-4357/acadd5](https://doi.org/10.3847/1538-4357/acadd5)
- Liakos, A., & Niarchos, P. 2017, *MNRAS*, 465, 1181, doi: [10.1093/mnras/stw2756](https://doi.org/10.1093/mnras/stw2756)
- Lianou, S., Grebel, E. K., & Koch, A. 2011, *A&A*, 531, A152, doi: [10.1051/0004-6361/201116998](https://doi.org/10.1051/0004-6361/201116998)
- Lightkurve Collaboration, Cardoso, J. V. d. M., Hedges, C., et al. 2018, *Lightkurve: Kepler and TESS time series analysis in Python*, *Astrophysics Source Code Library*, record ascl:1812.013. <http://ascl.net/1812.013>
- Liu, G. C., Huang, Y., Zhang, H. W., et al. 2020, *ApJS*, 247, 68, doi: [10.3847/1538-4365/ab72f8](https://doi.org/10.3847/1538-4365/ab72f8)
- Loumos, G. L., & Deeming, T. J. 1978, *Ap&SS*, 56, 285, doi: [10.1007/BF01879560](https://doi.org/10.1007/BF01879560)
- Lv, C., Esamdin, A., Hasanzadeh, A., et al. 2023, *The Astrophysical Journal*, 959, 33, doi: [10.3847/1538-4357/acf999](https://doi.org/10.3847/1538-4357/acf999)
- Lv, C., Esamdin, A., Pascual-Granado, J., Yang, T., & Shen, D. 2022, *ApJ*, 932, 42, doi: [10.3847/1538-4357/ac69d9](https://doi.org/10.3847/1538-4357/ac69d9)
- Lv, C., Esamdin, A., Zeng, X., et al. 2021, *The Astronomical Journal*, 162, 48, doi: [10.3847/1538-3881/ac082b](https://doi.org/10.3847/1538-3881/ac082b)
- McNamara, D. H. 2011, *AJ*, 142, 110, doi: [10.1088/0004-6256/142/4/110](https://doi.org/10.1088/0004-6256/142/4/110)
- Milligan, H., & Carson, T. R. 1992, *Ap&SS*, 189, 181, doi: [10.1007/BF00643125](https://doi.org/10.1007/BF00643125)

- Montgomery, M. H., & O'Donoghue, D. 1999, Delta Scuti Star Newsletter, 13, 28
- Mow, B., Reinhart, E., Nhim, S., & Watkins, R. 2016, AJ, 152, 17, doi: [10.3847/0004-6256/152/1/17](https://doi.org/10.3847/0004-6256/152/1/17)
- Murphy, S. J., Hey, D., Van Reeth, T., & Bedding, T. R. 2019, MNRAS, 485, 2380, doi: [10.1093/mnras/stz590](https://doi.org/10.1093/mnras/stz590)
- Murphy, S. J., Saio, H., Takada-Hidai, M., et al. 2020, MNRAS, 498, 4272, doi: [10.1093/mnras/staa2667](https://doi.org/10.1093/mnras/staa2667)
- Netzel, H., & Smolec, R. 2022, MNRAS, 515, 4574, doi: [10.1093/mnras/stac1938](https://doi.org/10.1093/mnras/stac1938)
- Otero, S. A. 2007, Open European Journal on Variable Stars, 0056, 1
- Petersen, J. O., & Christensen-Dalsgaard, J. 1996, A&A, 312, 463
- Pietrukowicz, P., Soszyński, I., Netzel, H., et al. 2020, AcA, 70, 241, doi: [10.32023/0001-5237/70.4.1](https://doi.org/10.32023/0001-5237/70.4.1)
- Poro, A., Paki, E., Mazhari, G., et al. 2021, PASP, 133, 084201, doi: [10.1088/1538-3873/ac12dc](https://doi.org/10.1088/1538-3873/ac12dc)
- Read, A. K., Bedding, T. R., Mani, P., et al. 2024, MNRAS, 528, 2464, doi: [10.1093/mnras/stae165](https://doi.org/10.1093/mnras/stae165)
- Ricker, G. R., Winn, J. N., Vanderspek, R., et al. 2015, Journal of Astronomical Telescopes, Instruments, and Systems, 1, 014003, doi: [10.1117/1.JATIS.1.1.014003](https://doi.org/10.1117/1.JATIS.1.1.014003)
- Samadi, R., Goupil, M. J., & Houdek, G. 2002, A&A, 395, 563, doi: [10.1051/0004-6361:20021322](https://doi.org/10.1051/0004-6361:20021322)
- Soszyński, I., Pietrukowicz, P., Skowron, J., et al. 2021, AcA, 71, 189, doi: [10.32023/0001-5237/71.3.1](https://doi.org/10.32023/0001-5237/71.3.1)
- Stassun, K. G., Oelkers, R. J., Pepper, J., et al. 2018, AJ, 156, 102, doi: [10.3847/1538-3881/aad050](https://doi.org/10.3847/1538-3881/aad050)
- Stellingwerf, R. F. 1979, ApJ, 227, 935, doi: [10.1086/156802](https://doi.org/10.1086/156802)
- Sun, X.-Y., Zuo, Z.-Y., Yang, T.-Z., Chen, X.-H., & Li, H.-R. 2021, The Astrophysical Journal, 922, 199, doi: [10.3847/1538-4357/ac323e](https://doi.org/10.3847/1538-4357/ac323e)
- Uytterhoeven, K., Moya, A., Grigahcène, A., et al. 2011, A&A, 534, A125, doi: [10.1051/0004-6361/201117368](https://doi.org/10.1051/0004-6361/201117368)
- Wils, P., Rozakis, I., Kleidis, S., Hamsch, F. J., & Bernhard, K. 2008, A&A, 478, 865, doi: [10.1051/0004-6361:20078992](https://doi.org/10.1051/0004-6361:20078992)
- Xue, W., Niu, J.-S., Xue, H.-F., & Yin, S. 2023, Research in Astronomy and Astrophysics, 23, 075002, doi: [10.1088/1674-4527/accdbc](https://doi.org/10.1088/1674-4527/accdbc)
- Yang, T.-Z., Sun, X.-Y., Zuo, Z.-Y., & Liu, H.-W. 2021a, AJ, 161, 27, doi: [10.3847/1538-3881/abcb8b](https://doi.org/10.3847/1538-3881/abcb8b)
- Yang, T.-Z., Zuo, Z.-Y., Li, G., et al. 2021b, A&A, 655, A63, doi: [10.1051/0004-6361/202142198](https://doi.org/10.1051/0004-6361/202142198)
- Ziaali, E., Bedding, T. R., Murphy, S. J., Reeth, T. V., & Hey, D. R. 2019, Monthly Notices of the Royal Astronomical Society, 486, 4348, doi: [10.1093/mnras/stz1110](https://doi.org/10.1093/mnras/stz1110)